Check for updates

Progress in the application of graphene-based nanomaterials for gas adsorption and mitigation of air pollution

Demilade T. Adedipe,[a] Ajibola A. Bayode [ID] *[b] and Odunayo T. Ore [ID] *[c]

Graphene-based materials (GBMs) have emerged as versatile and efficient candidates for gas adsorption and air pollution mitigation, particularly targeting CO_x, NO_x, SO_x, and volatile organic compounds (VOCs). This review highlights recent advances in the design and fabrication of GBMs, including green synthesis, heteroatom doping, and metal oxide hybridization. Emphasis is placed on emerging fabrication strategies that enhance porosity, surface chemistry, and gas selectivity. Notably, nitrogen-doped graphene has been shown to improve NO_x adsorption by up to 45%, while rGO–metal oxide composites demonstrate enhanced CO_2 selectivity under low humidity conditions. We analyse performance data trends and benchmark results from recent studies, outlining the key factors influencing adsorption efficiency. The sustainable development of GBMs using biomass and industrial waste precursors is also explored within the context of the circular economy. Finally, the review underscores the importance of integrating techno-economic analysis (TEA) into future research to support the scalable deployment of GBMs in industrial gas separation technologies.

1 Introduction

Rapid industrialization and urbanization in this modern era have been accompanied by various environmental and technological challenges. One of the notable problems is that of the surge in air pollution, climate change, and the disruption of the delicate balance of our ecosystem.[1] Numerous health challenges in humans and animals, particularly those related to the respiratory system, are linked to air pollution.[2] These respiratory diseases include Chronic Obstructive Pulmonary Disease (COPD), asthma, and bronchiolitis, as well as conditions like lung cancer, cardiovascular problems, and disorders of the central nervous system.[1,3,4] According to the World Health Organization (WHO), indoor air pollution is responsible for causing 4.3 million premature deaths, while outdoor air pollution has been identified as the cause of 3.7 million deaths annually.[5] In addition, the COVID-19 worldwide outbreak has increased the environmental burden and human susceptibility to prolonged exposure to indoor/outdoor air pollution, and the demand for improved air quality cannot be overemphasized.[6,7] Air quality does not only have negative effects on urban/rural dwellers; it is a critical determinant of plant health and

agricultural productivity. The physiological, morphological, and biochemical responses of plants are intricately influenced by air quality. From altering photosynthetic rates to impacting nutrient uptake, air pollution can profoundly influence the productivity and quality of agricultural produce.[8,9]

Air pollutants are classified based on their physicochemical features and consist of a heterogeneous mixture of suspended gases, liquids, and solids (Fig. 1). Combustion of fossil fuels and biomass, whether created artificially or naturally, is one source of air pollution.[10,11] Industrial processes, burning materials, automobile emissions, and ambient tobacco smoke are examples of man-made/anthropogenic sources of air pollution.[12] Volcanic ash, wildfires, different gases, and spontaneous secondary pollutants are examples of naturally occurring sources.[13,14]

Clean/pristine air should not contain pollutants ranging from suspended particulate matter to volatile organic compounds and heavy metals. These pollutants, including $PM_{2.5}$, PM_{10}, NO_2, SO_2, CO_2, CO, CH_4, polyaromatic hydrocarbons (PAHs), and heavy metals like Ni, Cd, As, and Pb, constitute human health risks and pose a significant threat to the ecosystems.[15,16] Studies conducted on animals and *in vitro* have demonstrated that exposure to allergens and air pollution together may have synergistic negative effects on allergic respiratory diseases.[17,18] Thus, the scientific world has focused on the development of advanced nanomaterials for the capture of hazardous materials and air cleanup in the last century.

The term "graphene" was proposed by the IUPAC commission to replace "graphite layers", which was inadequate for

[a]*State Key Laboratory of Marine Pollution, Department of Chemistry, City University of Hong Kong, Hong Kong, China*

[b]*Department of Chemical Sciences, Faculty of Natural Sciences, Redeemer's University, P.M.B. 230, 232101 Ede, Nigeria. E-mail: bayodea@run.edu.ng*

[c]*Department of Chemistry, Kogi State University, P.M.B. 222, Kabba, Nigeria. E-mail: oreodunayo@yahoo.com*
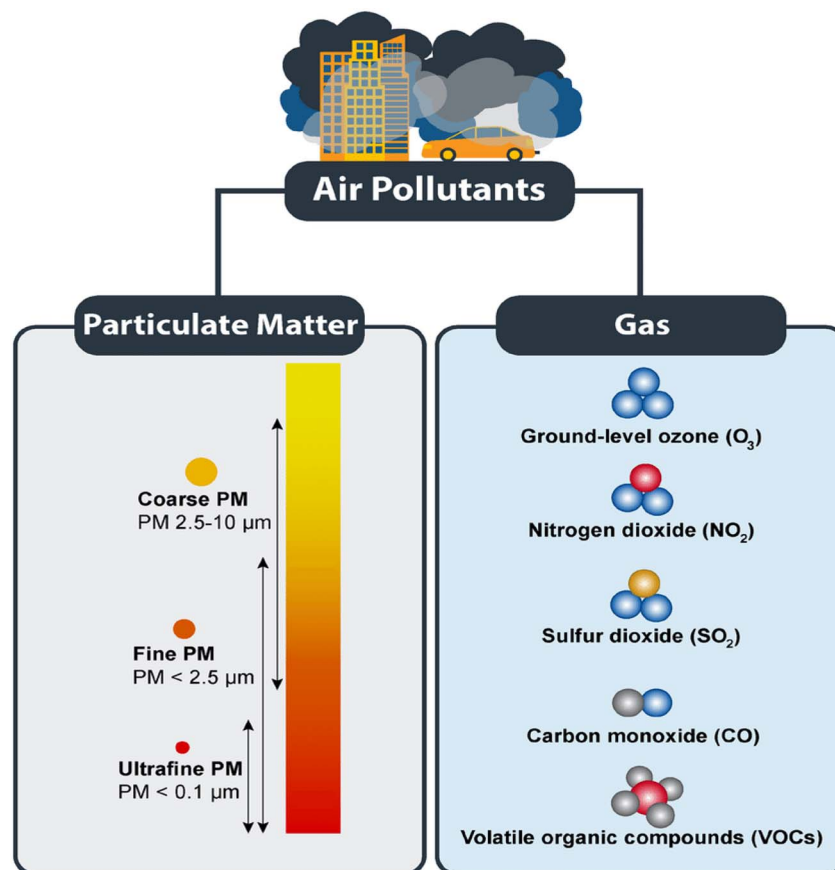
Fig. 1 Air pollution classification based on certain physical characteristics; PM stands for particulate matter. PM is divided by size into ultrafine, fine and coarse particles while gaseous pollutants include volatile organic compounds, carbon monoxide, sulphur dioxide, nitrogen dioxide, and ground-level ozone, all of which contribute to adverse health and environmental effects as well as the degradation of air quality.

studying single carbon layer structures, as "graphite" denotes a three-dimensional stacking structure. Graphene is now defined as a two-dimensional monolayer of carbon atoms, serving as the fundamental unit of graphitic materials like fullerene, nanotube, and graphite.[19–21] Despite graphite's ancient use dating back 6000 years for pottery decoration, research on graphene, essentially a single-atom plane of graphite, became more prominent in the 1960s when enhanced basal-plane conductivity was observed in graphite intercalation compounds.[22–24] This discovery sparked excitement in the scientific community, envisioning graphene as a lighter, cheaper alternative to metal conductors, yet uncertainty persisted regarding its high conductivity and future applications. Graphene research has progressed significantly in the last two decades, unveiling superior physicochemical properties in graphene layers and several composite forms.[25–28]

Significant advancements have been achieved in the development of graphene-based materials (GBMs) for a wide range of applications, particularly in gas adsorption technologies (see Fig. 2). As the diversity of GBMs continues to expand rapidly, there is an increasing need for a systematic and thorough comparison of functionalized GBMs in their efficacy for gas adsorption. This comprehensive review critically examines emerging synthesis strategies, including innovative approaches

such as chemical vapor deposition and liquid-phase exfoliation, while also addressing the inherent limitations present in current volatile organic compound (VOC) and carbon dioxide (CO_2) mitigation systems. Furthermore, the review identifies essential research directions aimed at overcoming these limitations, such as enhancing the selectivity and capacity of GBMs for targeted gas molecules, improving the scalability of production methods, and exploring novel functionalization techniques to optimize material properties for specific gas adsorption applications.

2 Overview of synthetic approaches for graphene-based materials

The graphene-based materials (GBMs) fabrication technique is one of the key aspects to take into account to maximize their architectural structure and hence boost their application, economic, and industrial value.[29] Specifically, GBM's unique characteristics, yield, micro/nanostructure, and overall quality profile are significantly influenced by the technique of fabrication, and establishing the best synthesis protocol has garnered attention from researchers from various fields.[29–31] By and large, the strategy of synthesizing GBMs is similar to that of carbon-
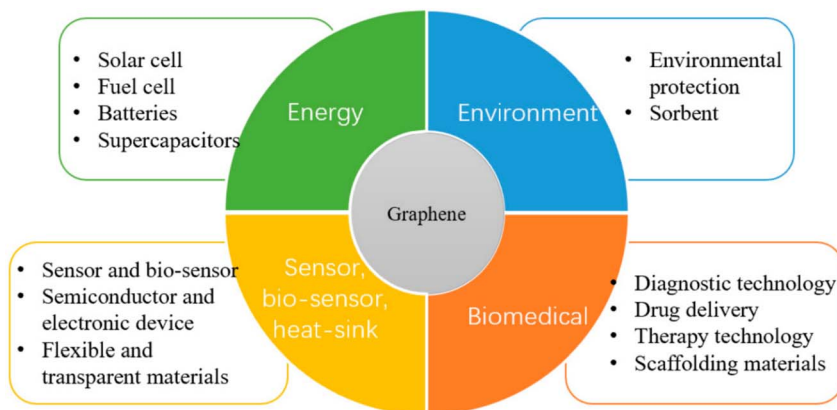
Fig. 2 Various fields of application of graphene/graphene-based materials. The exceptional properties of graphene make it useful in the energy, biomedical, and environmental sector as well as for heat-sink, biosensor, and sensor applications.

based nanomaterials, and it depends on various criteria such as the desired size of the product and nature of precursors. As shown in Fig. 3, the synthesis route can be classified into two categories; (1) top-down synthesis, also known as the destructive method and, (2) bottom-down synthesis, also known as the constructive method.[32] An in-depth overview of various synthetic approaches for GBMs is presented below.

2.1 Top-down synthesis of GBMs

Various methods are classified as top-down approaches in the synthesis of GBMs. These methods involve starting with larger structures or bulk materials and breaking them down into smaller components until graphene or graphene-like structures are produced.[33] Notably, the reduction of graphite oxide (–rGO),

Fig. 3 Overview of top-down and bottom-up graphene-based material synthesis route.

exfoliation (mechanical, electrochemical, and liquid phase), and the arc discharge technique are the most common top-down methods and are therefore usually employed for GBM fabrication.[29] In this sub-section, we will discuss different top-down approaches that can be used for GBMs.

2.1.1. Mechanical exfoliation (Scotch tape method). Mechanical exfoliation (MEX) is also known as micro-mechanical excision or the adhesive tape method. Historically, this Nobel prize-winning technique was the first approach that was developed for the fabrication of graphene as demonstrated by Geim and Novoselov in 2004. It involves the process of repeatedly peeling off layers of graphite using adhesive tape.[34] The adhesive force between the tape and the graphite overcomes the van der Waals force holding the layers of the graphene together, resulting in the formation of thin flakes of graphene.[35] In another study, tailored graphene was fabricated using wedge-based MEX of HOPG (highly oriented pyrolytic graphite).[36] In this study, molecular dynamics simulations demonstrated that the wedge position, cleaving rates, and boundary conditions were the main determinants of the shearing and folding of graphene layers (GLs). The layer folded when the wedge was positioned beneath 1/3 of the interlayer distance; when the wedge was positioned above these limits, the layers separated without folding. These outcomes demonstrated that simulations were useful in establishing the right parameters to produce certain kinds of graphene.

Notably, quite a few groups have reported that graphite (pristine) can be exfoliated to single-layer graphene devoid of defects using diverse solvents like benzylamine, ionic liquid, *N*,*N*-dimethylformamide (DMF), *N*-methyl pyrrolidone (NMP), *ortho*-dichlorobenzene, or water-surfactant solutions.[37,38] For instance, as illustrated in Fig. 4, Hernandez *et al.* showed that graphite can be dispersed and exfoliated in solvents like *N*-methyl pyrrolidone, whose exterior energy is comparable to that of graphene, allowing the graphite layers to be exfoliated because the solvent–graphene interaction balances the energy needed for the exfoliation.

While the mechanical exfoliation method is simple and effective for producing high-quality GBM (HQGBM), one issue
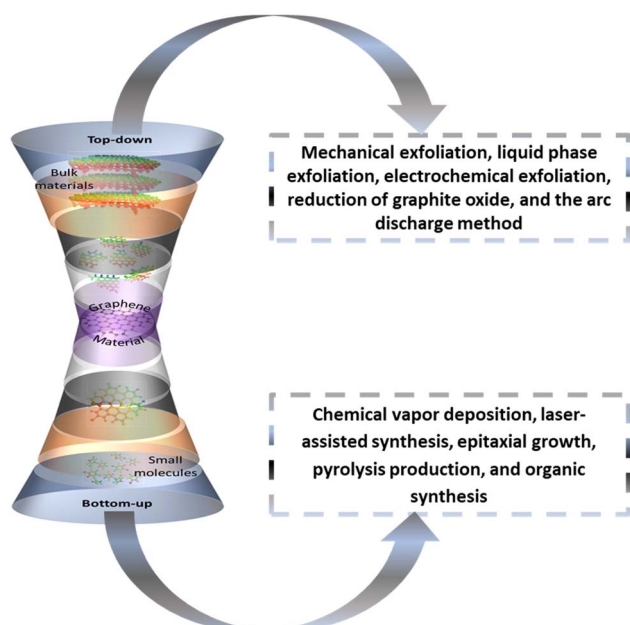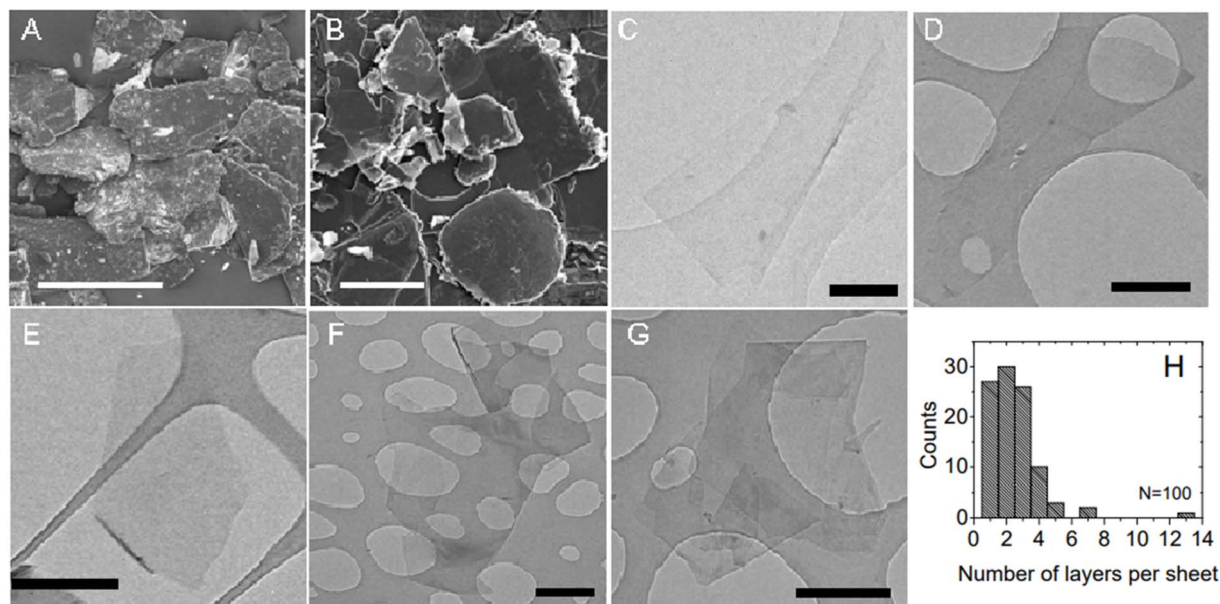
Fig. 4 (A) SEM picture of pristine graphite, (B) SEM picture of sediment following centrifugation, (C)–(E) bright field TEM picture of single-layer graphene flakes deposited from GBL, DMEU and NMP respectively, (F) a folded graphene sheet (bright field, deposited from NMP), (G) multi-layer graphene (bright field, deposited from NMP), (H) an NMP dispersions histogram showing the number of visual assessments of flakes as a function of the total amount of monolayers for each flake.[37]

with this approach is that the solvents that work well for this purpose frequently have high boiling temperatures, making it challenging to get rid of the solvents.[39] However, O'Neill's research team[40] posited that graphene can be exfoliated at greater concentrations with a thickness of fewer than ten layers in low-boiling point solvents like isopropanol and chloroform. In addition, this method suffers a major disadvantage which is low scalability and an inability to regulate the resulting graphene flakes' size and form.[35,41]

2.1.2. Liquid phase exfoliation (LPE). Historically, LPE was first introduced in 2008, and it is one of the most widely employed synthesis routes to produce graphene.[37] The process involves the dispersion of GtO or bulk graphite into a suitable solvent and ultrasonication or shear forces are applied to exfoliate the layers into graphene flakes, and the obtained graphene is purified[42,43] (Fig. 5). The LPE exfoliation of graphite depends on the mechanism of overcoming the van der Waals forces holding the GLs together. The commonly used solvents include water, organic solvents (*e.g.*, N-methyl-2-pyrrolidone, dimethylformamide), or surfactant solutions.[44] The choice of an appropriate solvent is hinged on the properties of the liquid like Hildebrand and Hansen solubility parameters, surface energy, and surface tension.

Yi and Shen reported that aqueous or non-aqueous solvents with surface energies (SE) within 70–80 mJ m^{-2} or surface tension within 40–50 mJ m^{-2} are good for graphite exfoliation because they match graphite surface energy of 46.7 mJ m^{-2}, due to the similarities in their SE to graphite ensuing in lesser mixing enthalpy, good wettability and simple exfoliation procedure.[46] The solvent should be able to overcome the van der Waals force from the interaction between GLs, which are held

within the π–π stacking distance of 3.35–3.4 Å.[47] As a result, dimethylformamide (DMF, 35.2 mJ m^{-2}), dimethylacetamide (DMA, 36.4 mJ m^{-2}), and N-methyl-pyrrolidone (NMP, 41.3 mJ m^{-2})[44] are often employed to exfoliate graphene. Solvents liquid phase exfoliation offers scalability and the ability to produce graphene dispersions, but the quality and yield of graphene can vary depending on the solvent and process conditions. Despite its many benefits, some studies have shown that sonication may result in flaws in the margins and basal planes of the GBM.[48]

2.1.3. Electrochemical exfoliation. Electrochemical methods involve applying electric potential to a graphite electrode submerged in an electrolyte solution. The electric field induces exfoliation of the graphite layers, leading to the formation of graphene in the electrolyte solution. Specifically, the idea behind the method is that species in the electrolyte migrate into the graphite's interlayer spacings when graphite electrodes are immersed in it and a steady voltage is applied. As a result, the van der Waals force between the graphite layers weakens and the graphite layers separate into distinct GLs.[49] As shown in Fig. 6, Graphite can undergo two different types of electrochemical exfoliation (ECEX): cathodic exfoliation, in which a −ve voltage is applied and cations from the electrolyte migrate to the graphite cathode, and anodic exfoliation, in which a +ve voltage is applied and anions from the electrolyte migrate to the graphite anode.[50]

More specifically, the ECEX of graphite is typically carried out in aqueous media, and the following are the primary procedures involved in this process:[50,51]

● Hydrolyzing water and generating O$_2$ and OH radicals.

● The transfer of O$_2$ and OH radicals to graphite and the opening of its edge.
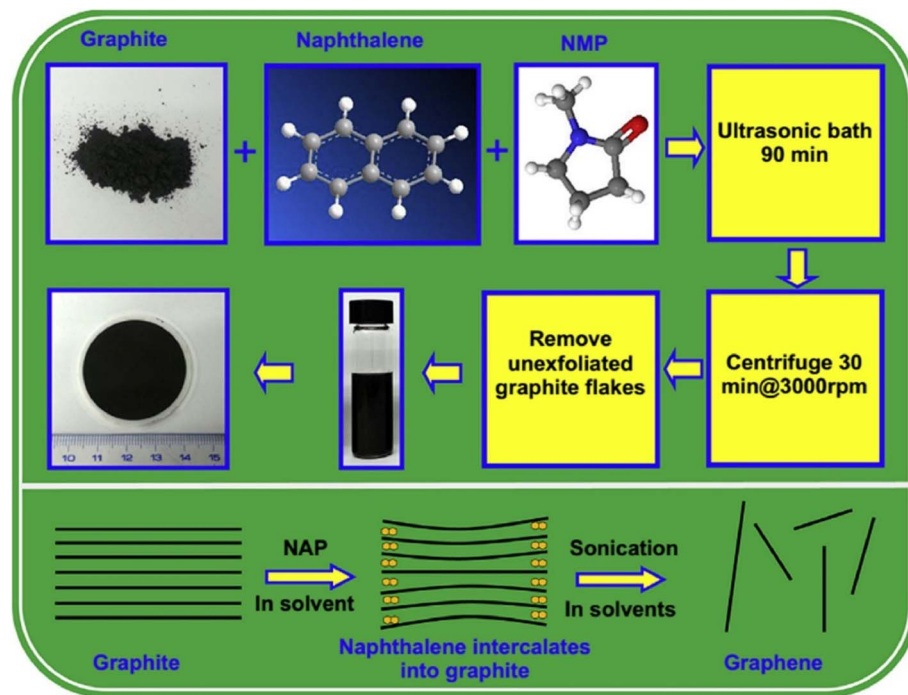
Fig. 5 Depicts the process of liquid-phase exfoliation (LPE) of graphite with the inclusion of naphthalene, comprising mixing, exfoliation, centrifugation, and vacuum filtration steps. Adapted with permission from ref. 45.

• The creation of gas as a result of the electrolyte species intercalating and expanding the graphite.

For instance, Parvez *et al.* explored the exfoliation of graphite in an H_2SO_4 aqueous solution.[52] To this purpose, they used a +10 V for two minutes to investigate the impact of H_2SO_4 concentration on exfoliation efficiency. The results indicated that 0.1 M H_2SO_4 had a higher exfoliation efficiency and yield than 1 M and 5 M H_2SO_4, most likely as a result of the more concentrated H_2SO_4 solutions producing bigger graphite particle pieces. On the other hand, exfoliation efficiency was decreased if the H_2SO_4 concentration was too low, most likely as a result of fewer anions. The scientists then looked at 1 : 1 H_2SO_4/acetic acid mixtures and pure H_2SO_4; in these instances, there was virtually little exfoliation and just a small amount of expansion. This demonstrated the worth of water in the electrochemical process as it may generate OH and O_2 radicals, which help with exfoliation and intercalation. The HQGBM that was exfoliated in a 0.1 M H_2SO_4 solution had a single sheet with a low sheet resistance of 4.8 kΩ per square, a large sheet size of around 10 μm, and a low oxygen concentration of 7.5 wt%.[52]

In another experiment, a straightforward electrochemical process for creating graphene/α-MoO_3 composites was described by ref. 53. High-purity graphite rods, PTFE, sodium dithionite, potassium hydroxide, and sodium molybdate were utilized. In this research, an electrolysis cell containing 40 mL of 0.2 M sodium molybdate as the electrolyte was filled with two graphite rods. After applying a static potential of 10 V for 30 minutes, the anode graphite rod began to corrode. Subsequently, 0.15 grams of $Na_2S_2O_4$ were introduced into the electrolyte to adjust the pH level. After two hours, the α-MoO_3 GBM

was removed from the reactor and cleaned in ethanol and deionized water until the pH reached neutrality. Afterward, they were dried for twelve hours at 60 °C in an oven. The α-MoO_3 GBM was subsequently annealed at 200 °C in the air for two hours before being cooled to ambient temperature to produce a suitable conductive material. Their findings demonstrated that the α-MoO_3 GBM has high thermal performance and that the α-MoO_3 NPs are evenly dispersed on the surfaces of graphene sheets (GSs). Fig. 7 provides a schematic representation of the single-step ECEX and functionalization of graphene with α-MoO_3. The MoO_4^{2-} anions migrate to the graphite anode when the anodic voltage is applied, and in very acidic circumstances, MoO_4^{2-} intercalates into the graphite underlayers and transforms into α-MoO_3. Then, graphene/α-MoO_3 composites are formed as a result of the exfoliation events.[53]

In another study, different amounts of zinc nitrate in an electrolyte solution were utilized to create a variety of zinc oxide/graphene (ZnO/Gr) nanocomposites *via* an electrochemical exfoliation process. The authors found that ZnO/Gr nanocomposite produced using 7 mmol of zinc nitrate displayed a sheet-like morphology with an even decoration of ZnO NPs over the GSs, and was more effective in dye degradation application.[54] Similarly, Kotkin *et al.* exfoliated cobalt and placed it surface of graphene utilizing the ECEX approach aided by plasma. Combining the 0.01 M $CoSO_4$ solution with the 1 M Na_2SO_4 solution produced the utilized electrolyte. For ten hours, an alternating +300 V (anodic) and −150 V (cathodic) was employed Cobalt is deposited on the cathode's surface during the anodic mode of operation. The deposited cobalt particles are then dissolved in the cathodic type operation which
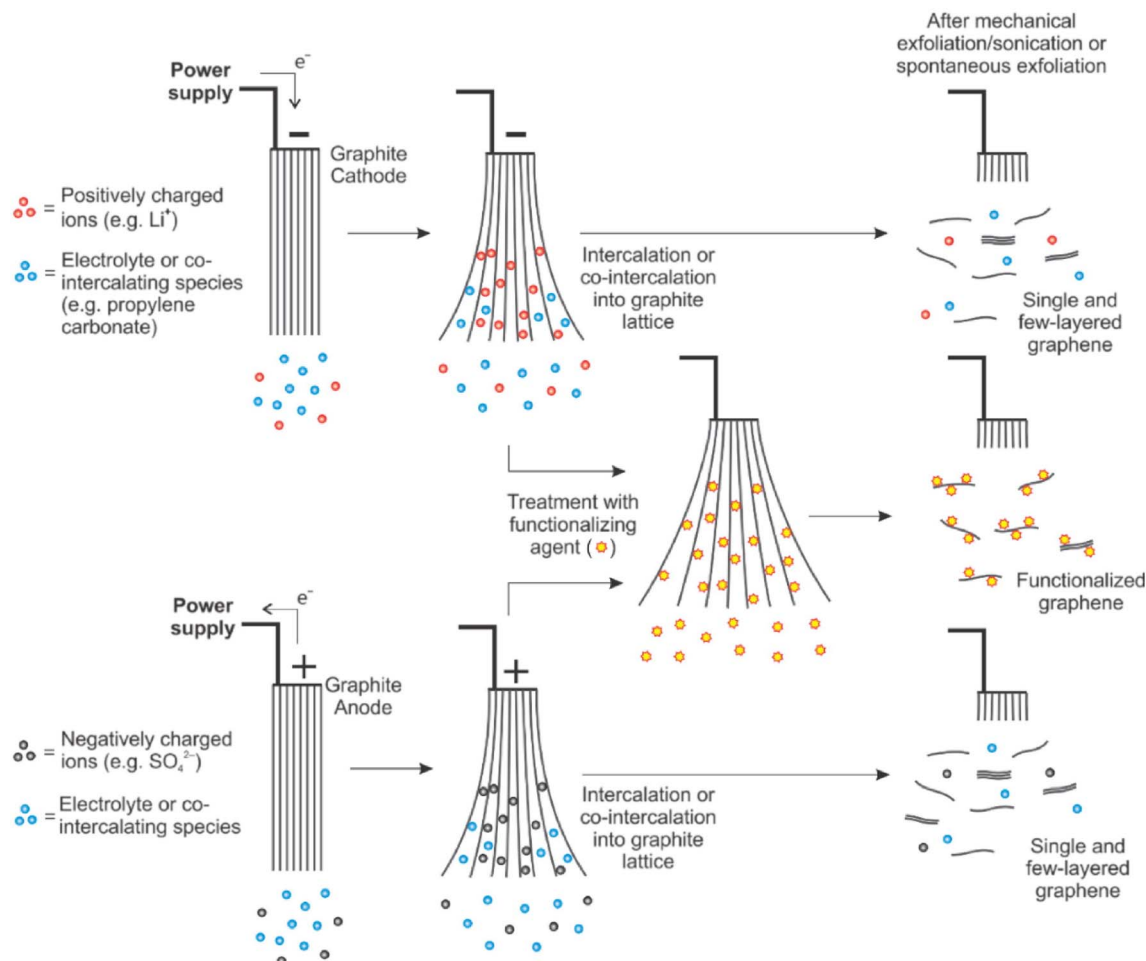
Review

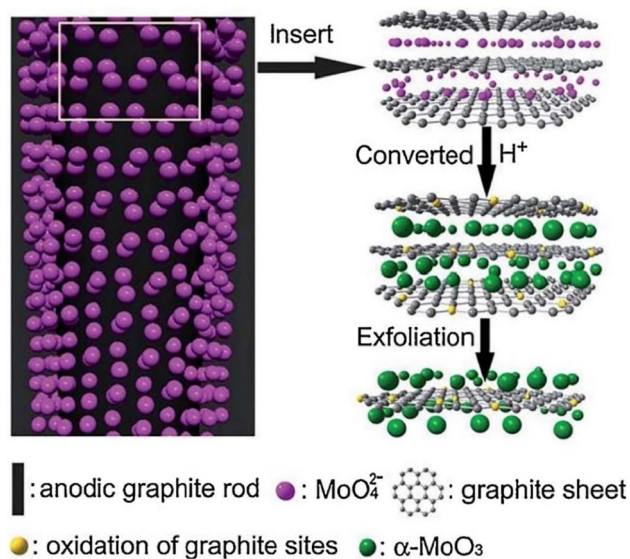Fig. 6 Mechanistic synopsis of anodic and cathodic electrochemical exfoliation.[51]

Fig. 7 Plausible mechanism for the synthesis of α-MoO₃ GBM by the ECEX process.[53]

produces the graphene/cobalt oxide composites.[55] Motta's research team[56] employed sonication for anodic ECEX of HOPG in an aqueous solution of sodium dodecyl sulfate and Na_2SO_4 electrolyte. It was discovered that the system with sonication generated largely four-layer graphene flakes, whereas the system with sonication supplied primarily bilayer graphene flakes. Additionally, sonication-assisted graphene sheet production yields higher-quality results than the non-sonication approach, as demonstrated by Raman spectroscopic observations. This is probably because graphite may be exfoliated more easily by ultrasonication, which shortens the period that graphite is intercalated and oxidized. Consequently, there may be a decrease in C–OH and C=O oxygenated functional groups and defects.

In another study, Parvez and colleagues explored the exfoliating effects of a range of inorganic salt aqueous electrolyte solutions in anodic exfoliation, including $(NH_4)_2SO_4$, K_2SO_4, $NaNO_3$, NH_4Cl, Na_2SO_4, and $NaClO_4$.[57] Notably, sulfate ions (SO_4^{2-}) were discovered to have superior exfoliation efficiency compared to other anions. Investigations were also conducted on the impact of electrolyte concentration in the $(NH_4)_2SO_4$ system. At concentrations below 0.01 M, less than 5 weight

percent of the initial graphite was exfoliated. A yield of greater than 75 weight percent was obtained at concentrations up to 1 M. Nevertheless, because of the low water content and reduced graphite edge oxidation at concentrations of 3 M and 5 M, less than 50 percent yield was realized. In this study, it was discovered by the authors that ideal settings were 0.1 molar aqueous solution of $(NH_4)_2SO_4$ with a +10 V. Under these circumstances, over 85% of GSs exhibit three layers or less, while over 80% exhibit a lateral dimension greater than five µm. About 44 µm was the biggest graphene sheet that was found using SEM. The I_D/I_G ratio was found to be 0.25 *via* a Raman spectroscopy investigation, which is significantly less than chemically reduced GO. The exfoliated graphene seemed to have a 5.5% oxygen content, according to XPS measurements. Additionally, the generated graphene demonstrated outstanding hole mobility of 310 cm^2 V^{-1} s^{-1}.[57]

Similarly,[58] devised a facile technique that utilized anodic exfoliation of graphite in a mild $NaOH/H_2O_2/H_2O$ system. Exfoliation in this system is mostly dependent on H_2O_2, with exfoliation efficiency rising sharply between 0 and 130 mM H_2O_2 concentrations. The ideal exfoliation conditions were 3 M NaOH, 130 mM H_2O_2, and a working voltage of 1 V for ten minutes at room temperature, followed by 3 V for ten minutes. Under these circumstances, 95% of the high-quality GSs with three to six layers were formed. The product's I_D/I_G, a measurement of graphene flaws, was 0.67 in the Raman spectra as opposed to 0.54 for graphite. The introduction of oxygenated functional moieties during the ECEX process, which results in disorder at carbon edges, is what drives the rise in I_D/I_G.[59,60] By and large, the electrochemical exfoliation approach offers a simple, fast, and scalable method for producing graphene, but the quality of the obtained graphene can vary depending on the electrolyte composition and process parameters.

2.1.4. Reduction of GtO using chemicals and phytochemicals. Graphene can by synthesized by reducing GtO *via* a process that selectively removes oxygenated functional groups (OFGs) such as carbonyl (C=O) groups as a form of recovering the sp^2-hybridized carbon skeleton, to a limited extent.[61] Nonetheless, it is beneficial that these OFGs are found to be present on GO, and their tunability makes it useful in many applications, such as gas adsorption, because it helps to increase the surface reactivity and enable molecular interactions.[62,63] Specifically, reductants such as sodium hydrosulfite have been used to successfully produce various GBMs at relatively low temperatures in a matter of few minutes. For example, Guex's research group published a low-cost aqueous reduction technique based on sodium borohydride to prepare graphene. The wide-range diminution of C–O moieties (such as epoxy and hydroxyl) in the GtO during the early stage was accomplished by using a 300-mM aqueous solution of borohydride at 80 °C. This gave the graphene product good electrical conductivity, which progressively increased to 1500 S m^{-1} during the residual reaction time.[64] Similarly, sodium hydrosulfite was employed to reduce GtO as an effectual reductant. The findings show that sodium hydrosulfite may reduce GtO to a degree similar to that of hydrazine in a matter of minutes. It offers a productive way to

minimize GtO and may be applied to the creation of cutting-edge composites.[65,66]

In addition, the reductive process of GO is an essential process that is used in the restoration of the electrical conductivities and modification of the surface chemistry for specific usage.[67] Although chemical reducers such as hydrazine hydrate and sodium borohydride can do the same task, they are very hazardous to the environment and to human health. On the contrary, ascorbic acid (vitamin C) has recently become a green non-toxic and biocompatible alternative material for the reduction of GO. Recently, it has been shown that the reduction of GO in mild conditions under the catalytic effect of L-ascorbic acid can be effective and that the resultant reduced graphene oxide (rGO) has greatly improved electrochemical properties and an insignificant environmental burden.[67,68] It should, however, be noted that concentration that is too high may lead to partial reoxidation of rGO. Hence, there is the need to optimize reaction conditions in order to maintain the reduction efficiency.[67]

In recent times, solvothermal reduction and bioreduction methods using biogenic resources have been employed in material synthesis.[69–72] For example, as shown in Fig. 8,[73] present a simple and effective method for producing highly-rGO (*P. glutinosa*-HRGO) through the bio-reduction of GtO with plant extract from *Pulicaria glutinosa*. In addition to reducing GtO, the phytomolecules[74–76] in the *P. glutinosa* extract also functionalize the biogenic HRGO nanosheets' surface and stabilize them in a range of solvents, reducing the need for additional, potentially hazardous chemical reductants and surfactants. By making biogenic HRGO with varying concentrations of *P. glutinosa*, the impact of *P. glutinosa* on its dispersibility in different solvents was examined. The dispersibility of biogenic HRGO was then contrasted with that of chemically rGO. The biogenic HRGO was of higher quality than chemical RGO[73] owing to the various phytochemicals present in the biogenic extract.[32,77,78] GtO reduction, like liquid phase exfoliation, may achieve large-scale graphene fabrication;[29] however, this method is somewhat constrained by intricate procedures and structural flaws, as well as presenting environmental concerns.

2.1.5. Ball milling technique. The process of ball milling involves grinding graphite or GtO in the presence of a solvent, with the aid of a grinding agent (such as steel balls). The mechanical forces during milling cause the layers of graphite to exfoliate into graphene. Exfoliation of graphene occurs due to both normal and lateral forces. The balls in the milling process collide with the surface of GSs, leading to exfoliation induced by normal forces. However, if the normal forces are too high, the crystalline structure of the sheets can be damaged, leading to fragmentation instead of exfoliation. To avoid this, a balance needs to be struck between the normal and shear forces applied. Reducing normal forces while ensuring that shear forces are dominant and strong enough to overcome van der Waals forces can achieve this balance. Generally, there are two forms of ball milling: dry ball milling where inert water-soluble inorganic salts are employed, and wet ball milling, which uses solvents.[32,79] For example, Zhao *et al.* reported on the production
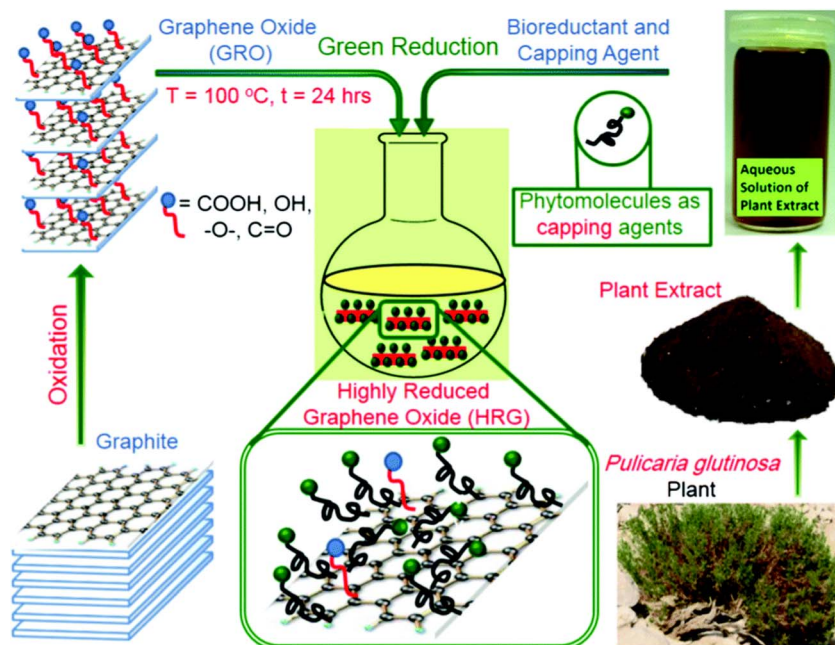
Fig. 8 Reduction of GtO utilizing an aqueous extract of the *P. glutinosa*.[73]

of crystalline GSs by exfoliating graphite platelets in a liquid media by wet ball milling. In this study, to establish the range of shear stress, 0.02 grams of few-layered nano graphite sheets were evenly spread within 80 millilitres of dry DMF at a concentration of 0.25 milligrams per millilitre. Subsequently, the GNs underwent exfoliation *via* ball milling dominated by shear force for 30 hours using a planetary mill containing zirconia balls and poly(tetrafluoroethylene) containers, operating at a gentle pace of 300 rpm. Large particles were taken out of the dispersion using a centrifuge. The thickness of the cross-section was determined to be between 0.8 and 1.8 nm, which is equivalent to the thickness of around three layers in single- and few-layer graphene.[80]

In another study, Lv *et al.* reported dry ball milling for the fabrication of graphene nanosheets. In this study, the authors used the soluble salt-assisted method to manufacture graphene nanosheet powder.[81] A stainless-steel jar containing 50 g of Na_2SO_4 powder, and some graphite was subjected to a 24-hour ball milling process at 150 rpm. As the ratio of Na_2SO_4 was increased, the number of layers rapidly dropped to bi-layers from multi-layers. Similarly, Lin's research group[82] employed a ball milling technique combined with shear force to grind elemental sulfur, which aids in exfoliation and attachment onto GSs in a structure with 73 wt% sulfur. The research group developed high crystalline GSs by using sulfur, a substance that is somewhat sticky for the graphite plane, as a substitute for Scotch tape. Ball milling is a scalable and simple method for producing graphene, but the process parameters must be carefully controlled to prevent contamination and damage to GSs.

2.1.6. Arc discharge method. The arc discharge (ADC) is the oldest of the best methods for fabricating high-quality carbon-

based materials including carbon nanotubes, and graphene-based materials.[83] The ADC approach was initially employed by Krastchmer and Hoffman. This technique uses an electric arc oven that has two graphite electrodes and a steel chamber that is cooled by water. As seen in Fig. 9, an additional direct current arc voltage is delivered across the two graphite electrodes while they are submerged in an inert atmosphere. For instance, Wu *et al.* successfully produced around 2.1 g of high-quality GSs on a wide scale using an enhanced alternating current ADC process under nitrogen and hydrogen mixed buffer gasses, and the arc-discharge duration was less than 5 minutes.[84] With no more than five layers, the as-prepared GSs show a low-defect structure. It is believed that nitrogen and hydrogen gases are both necessary for the creation of superior GSs. Additionally, based on the research findings, the volume ratio of nitrogen to hydrogen may have a significant role in minimizing the defects and layer counts of GSs.[84] In contrast to chemical techniques, the graphene fabricated exhibited lower structural flaws and was more readily dispersible in organic solvents, which improved its potential usage.

Similarly, Cheng *et al.* employed a vacuum ADC approach integrated with a high-temperature furnace was used to synthesize graphene on copper foils. By combining the benefits of vacuum ADC with chemical vapour deposition, SLG may be produced at a base temperature of 600 °C using a tiny furnace.[86] The substrate surface can then be quickly heated to 1100 °C using photon radiation from the vacuum arc. Through a series of studies on processing time, arc currents, cooling, and ambient pressure, the ideal fabrication condition was found. SEM, Raman spectroscopy, and optical microscopy observations revealed that the principal products were SLG, which has a consistent thickness across the substrate. The findings
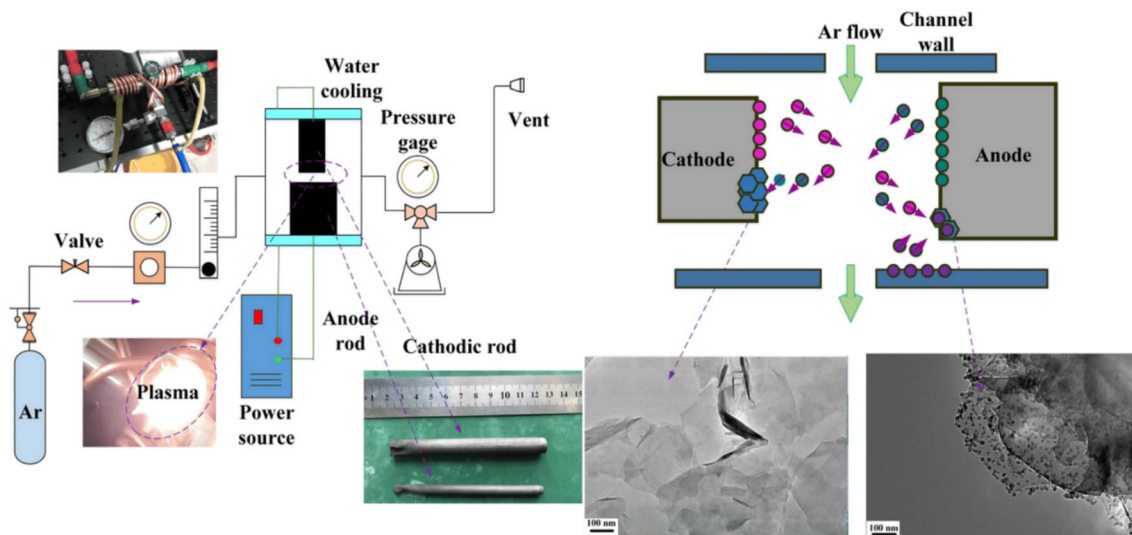
Fig. 9 Diagrammatic depiction of the arc discharge process used for fabricating graphene.[85]

showed that a simple and inexpensive way to synthesize GSs for graphene-based applications is to combine a vacuum arc with a thermal approach that employs graphite as a carbon source.[86]

In another study, an ideal He ADC approach uses an 80 A current and 550 torr of He atmospheric pressure to fabricate GSs. The result shows that single-layer, double-layer, and few-layer GSs were produced.[87] In a similar study, Kim's team[88] demonstrated that high-quality BLG and FLG could be produced with fewer layers of graphene by using the aqueous ADC technique; the mean lateral diameters of these products ranged from 4.4 to 28.3 μm. The interlayer gap was preserved at around 0.34 nm for every level of the ADC power, and the regulation of the quantity of GLs stacked was achieved by adjusting the power of the ADC. Notably, in contrast to earlier research, the arc-discharge approach was used by ref. 89 to study the development processes of FLG under real production settings including He, O–He, and H–He. The production of a few layers GSs with lateral widths ranging from 50 to 300 nm was seen exclusively in the presence of reactive gases. This finding may suggest that the growth process of FLG involved the evaporation of graphite followed by the reactive gas-confining crystallization of the evaporated carbon clusters. The major advantage is that the ADC approach is an eco-benign and inexpensive technique that can effectively fabricate HQGBM in relatively high yields.[90,91] However, this method has the disadvantage of carbonaceous impurities.[92] Since the kinds of buffer gases and arc parametric settings affect the quality of graphene, additional adjustment of these factors is necessary to increase the effectiveness of the preparation process.[29] Therefore, more investigation into the fundamental mechanics behind the synthesis of graphene is needed for a more in-depth understanding of process parameters and techniques required to obtain desired graphene morphology and physicochemical properties.

2.2 Bottom-up approach for GBM synthesis

Bottom-up approaches in material synthesis refer to procedures where materials are built from atomic or molecular components, building up to larger structures or assemblies. By and large, this technique usually involves the self-assembly or chemical synthesis of smaller entities at the atomic or nanometer scale.[60,93] Specifically, in bottom-up approaches, the control over the architectural arrangement and properties of the final material often arises from the interactions and properties of the smaller components. More specifically, most bottom-up methods for manufacturing graphene depend on using hydrocarbons as precursors.[29,94] Some bottom-up methodologies for graphene preparation are presented in this section.

2.2.1. Chemical vapour deposition (CVD). CVD is a controllable and effective synthetic method that produces HQGBM materials in large quantities by growing it on metal surfaces or substrates like silica,[95] Cu,[96] Ni,[77] Au,[72] Mo,[97] Ir,[98] and Pt.[99] Notably, in recent years, the preparation of GBM using the CVD route has significantly advanced and different CVD methods have been developed.[100] In 2011, Chen et al. for the first time developed a generic approach for the fabrication of 3D graphene foam (GF), by template-assisted CVD technique.[101] In this study, a template consisting of Nickel foam with a 3D macroporous structure that is interconnected was selected, as seen in Fig. 10. By pyrolyzing CH_4 at 1000 °C and ambient pressure, GSs were precipitated on the surface of Ni foam. The Ni skeleton was then etched off using a hot HCl (or $FeCl_3$) solution. A thin coating of poly(methyl methacrylate) was put on the graphene surface as a support to stop the graphene network from collapsing while etching. A monolith of continuous and linked graphene 3D network was created after the poly(methyl methacrylate) was removed using hot acetone. The freestanding 3D GF is pliable, and very light, weighing just 5 mg cm^{-3}, with good specific surface area (SSA) of up to 850 m^2 g^{-1}.

Following the report of Chen's team,[101] various researchers[102-104] have employed diverse carbon sources and or reaction conditions to synthesize high-quality three-dimensional GBMs using the template-assisted CVD technique. For instance, Liu's group[104] produced a graphene film with great crystallinity by using asphalt as a carbon source. In
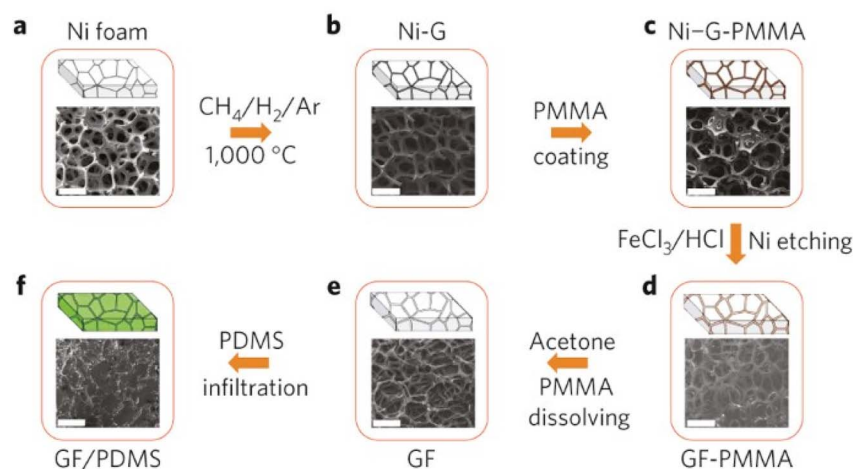
Fig. 10 (a–f) Showing the different stages of the fabrication of a graphene fibre and integration with PDMS.[101]

this research, after one hour of immersion in the asphalt-toluene solution, the cleaned Ni foam was dried. The Ni foam encased in asphalt was put in the middle of the tube furnace and given a 10-minute breakdown treatment at 940 °C and 1.5×103 Pa. After the NF was removed by etching, graphene foam made up of two to five layers of GSs was produced. In another experiment, Kim's group[105] employed the CVD approach to produce graphene on commercial 3D Cu foam (CF). To preserve the 3D structure, a poly(methyl methacrylate) layer was spin-coated on the 3D graphene/CF. After chemically etching the CF out of $(NH_4)_2S_2O_8$ solution (1 wt%), a 3D GBM was produced.

Conversely, Wei's group[106] fabricated a 3D graphene network without needing a solvent. In this study, CF was first obtained by annealing Cu powder at 1000 °C with 200 sccm H_2. Next, using the CVD process, GLs were produced on this 3D Cu foam. By using a high-temperature evaporation procedure to take out the Cu template, a 3D graphene network was created without the need for a solvent process. In another study, rapid thermal CVD produced around 12.31% more graphene domains than thermal CVD did.[107] Another work by Liu's group[108] used naturally occurring scallops as the raw material to create a low-cost, readily removable CVD template. The scallop was heated in the air to produce a very porous CaO framework. Next, using the CVD process, GLs are developed on the constructed framework. After the CaO was finally etched in diluted HCl and freeze-dried, a self-supporting 3D GF was produced. Also, HQGBM with several layers was synthesized on Cu–Ag alloy powder by *in situ* CVD at 900 °C by ref. 100. In another study, by allowing carbon atoms to diffuse through the nickel template, Xu's research team[109] synthesized a centimetre-scale, extended SLG on a Ni surface placed on a highly oriented pyrolytic graphite substrate. Their findings show how to optimize the temperature and annealing time, two critical factors for graphene formation, to produce precise control over the degree of thickness and structure of the GLs.

In another investigation, the significance of kinetic variables in the CVD preparation of homogenous large-area graphene utilizing Cu catalyst has been explored by ref. 110. It was discovered that at low methane concentrations (ppm), graphene grew as a monolayer, and at higher concentrations (5–10% by volume), it formed multilayers at atmospheric pressure. Another research group[111] shows the use of centimetre-scale Cu substrates as a novel path for the industrial-scale fabrication of high-quality GSs. This efficient, time- and money-saving roll-to-roll approach yielded 30-inch GSs while also offering a large-scale, high-quality, and productive graphene synthesis for real-world use. Although, the CVD method is effective and controllable as stated earlier.[29,112] Nevertheless, it is extremely difficult to precisely manage graphene's edge structure and topology.[39] Additionally, when CVD GBM is formed on catalytic metal substrates like Pt and Ir, defects can occur.[98] Hence, to control the grade of the GBM, it is crucial to adjust preparation parametric conditions including growth temperature, working pressure, deposition duration, substrate type, and flow frequency of H gases and C precursor appropriately.

2.2.2. Epitaxial growth method. The epitaxial fabrication of graphene on SiC wafer surfaces *via* SiC breakdown and Si desorption from the surface is another popular technique for graphene production.[39] In this method, through carefully regulated sublimation, the carbon-rich surface is rebuilt and graphitized to produce graphene islands throughout the SiC wafer surface.[113] For instance, Berger's group[113] produced ultrathin epitaxial graphite films in 2004 that were only a few monolayers thick. Thermal desorption of Si resulted in the production of epitaxial graphene on the Si-terminated face of single-crystal 6H-SiC. To remove the oxide, samples were etched with H_2 and heated in an ultrahigh vacuum under electron bombardment. Tens of nanometer-sized few-layered EG films, usually consisting of three GSs, were produced. Temperature was the primary determinant of layer thickness. Similarly, Rollings's research team[114] synthesized GLs on an n-type 6H-SiC single-crystalline wafer's Si-terminated face. After the samples were placed in an ultrahigh vacuum preparation room, surface oxides were removed *in situ* by annealing them for 20 to 30 minutes at 850 °C with silicon flux. It was possible to create

atomically thin EG with thicknesses as low as 1–2 GLs and a few microns.

In a more recent study, a four-inch single-crystal monolayer graphene wafer grew on $Cu_{90}Ni_{10}$ film owing to the substantial increase in catalytic activity of trace Ni, and this growth process occurred fifty times more quickly than on Cu.[115] Furthermore, many research teams have created alternative EG growth methods to produce larger and better-quality graphene.[60] For example, in place of the previously employed vacuum breakdown of SiC, Emtsev *et al.* described the fabrication of single-layer GSs with greater domain sizes (3×50 μm^2) using an *ex situ* graphitization of Si-terminated SiC at argon atmosphere under 900 mbar.[116] They have improved the control rate of Si sublimation using this novel method, which has improved the material's surface morphology. In like manner, through the development of an alternative growth approach, De Heer and his colleagues[117] were able to regulate the Si sublimation by encasing the SiC crystals in graphite enclosures. They prevented Si from escaping, resulting in a high Si vapour pressure and excellent control over the graphitization temperatures. Consequently, they were able to create homogeneous GLs of excellent quality on both the C-facing and the Si-terminated face of the SiC single crystal. The epitaxial growth method and the result obtained by ref. 117 are similar to the one reported by ref. 118 but by adopting a Si flux approach that used disilane gas to manage the Si vapour pressure, which improved graphene's quality.

Notably, the following are the main benefits of epitaxial growth: (i) the material produced may be guided by properly tailoring the substrate; (ii) there are no trapped contaminants beneath the graphene, and (iv) the material does not need to be transported from the metal to another dielectric substrate.[39] Nevertheless, the primary constraints of this technique are the high temperature employed throughout the procedure and its non-transferability to alternative substrates. Hence, further investigation is needed into the proper substrate choice and how it affects the growth and crystalline quality of graphene.

2.2.3. Organic synthesis. In recent years, a technique of producing graphene by organic synthesis has been proposed as a special bottom-up approach, wherein discotic aromatic hydrocarbons with certain chemical structures and functional groups are used as precursors.[119,120] For example, as shown in Fig. 11, Yang's team[121] developed a bottom-up organic synthesizing method for synthesizing soluble GNRs that are very small (about 0.5 nm) and using a nonoxidative-alkyne-benzannulation technique supported by Brønsted acid. The GNR precursor, poly(2,6-dialkynyl-*p*-phenylene) (PDAPP), with a weight-average molecular weight of 37.6 kg mol^{-1}, was created by Suzuki polymerization. Brønsted acids were effectively used to cyclize the ethynylaryl side chains on PDAPP, which resulted in the production of GNRs.

Furthermore, a variety of nanographenes with different architectures and thicknesses may be synthesized by adjusting the structure of the precursor monomers.[122,123] For example,[122] propose a surface chemical pathway that makes it possible to synthesize customized nanographenes from polyphenylene precursors with atomic precision. Scanning tunnelling microscopy and density functional theory are used to study the cyclodehydrogenation of a typical polyphenylene on Cu. The research findings provide unheard-of insight into a dehydrogenative intramolecular aryl–aryl coupling process. The authors discover that thermally driven cyclodehydrogenation occurs *via* many intermediary stages, two of which may be stabilized on the surface. Unfortunately, the main issue in the field of organic synthesis of nanographene is how to practically process large polycyclic aromatic hydrocarbons (PAHs).

Specifically, it has been discovered that strong intramolecular π–π interactions lead PAHs bigger than hexabenzocoronene to be insoluble in organic solvents or sublimable without crumbling.[124] Interestingly, it has been accentuated that bringing the long, flexible aliphatic chains to the edge of the planar nanographene is one method of solubilizing the nanographene.[125,126] Nevertheless, this strategy becomes less effective as graphene gets bigger, thus the need to develop novel approaches to address this issue. Sun *et al.* attempted to address this setback by using a metal catalyst substrate and a temperature of 800 °C to deposit large areas of HQGBM with controllable thickness without the use of aromatic polymers.[127] The organic synthesis technique is a useful addition to CVD growth as it allows for relatively low-temperature development and gets around the CVD method's constraint on the use of gaseous ingredients. However, graphene's large-scale production is limited by the comparatively high cost of the organic synthesis route.

2.2.4. Laser-assisted method. Laser-aided processing methods have arisen as robust tools in several applications.[60,128] The manufacturing of graphene at a cheap cost and with rapid development is possible with the use of laser-aided synthesis. There are two main categories of laser-assisted graphene fabrication techniques. While one approach is similar to the CVD process, wherein a laser is used to dissolve the carbon in the metal when the precursor is exposed to light. Graphene is created when the carbon precipitates on the metal surface after cooling.[129,130] The second type of laser-assisted graphene fabrication technique causes photothermal and photochemical changes on the substrate through the application of lasers to generate the product. Also, laser-aided graphene fabrication can be carried out in ambient air in the absence of solvents, which is beneficial for several commercial-scale applications.[29]

For example, Lin and colleagues employed a CO_2 infrared laser to directly scribe commercial polymer films, yielding porous graphene films with intricate three-dimensional structures. They also utilized a fast and versatile laser reduction technique on GO, enabling the direct formation of graphene on solid surfaces with submicron dimensions, without the need for chemicals.[131] In 2020, Stanford and co-workers[132] developed laser-induced graphene (LIG) by utilizing a visible 405 nm laser, connected to a fibre with a low power of roughly 161 mW, a diameter of about 3 μm, and a pulse duration ranging from 2 μs to 100 ms, on a polyimide (PI) surface. By positioning this laser setup atop an SEM chamber, they observed the real-time formation of laser-induced graphene through secondary electron imaging. A minimum fluence of 83.4 J per cm^2 per pulse was necessary to generate laser-induced graphene. The process
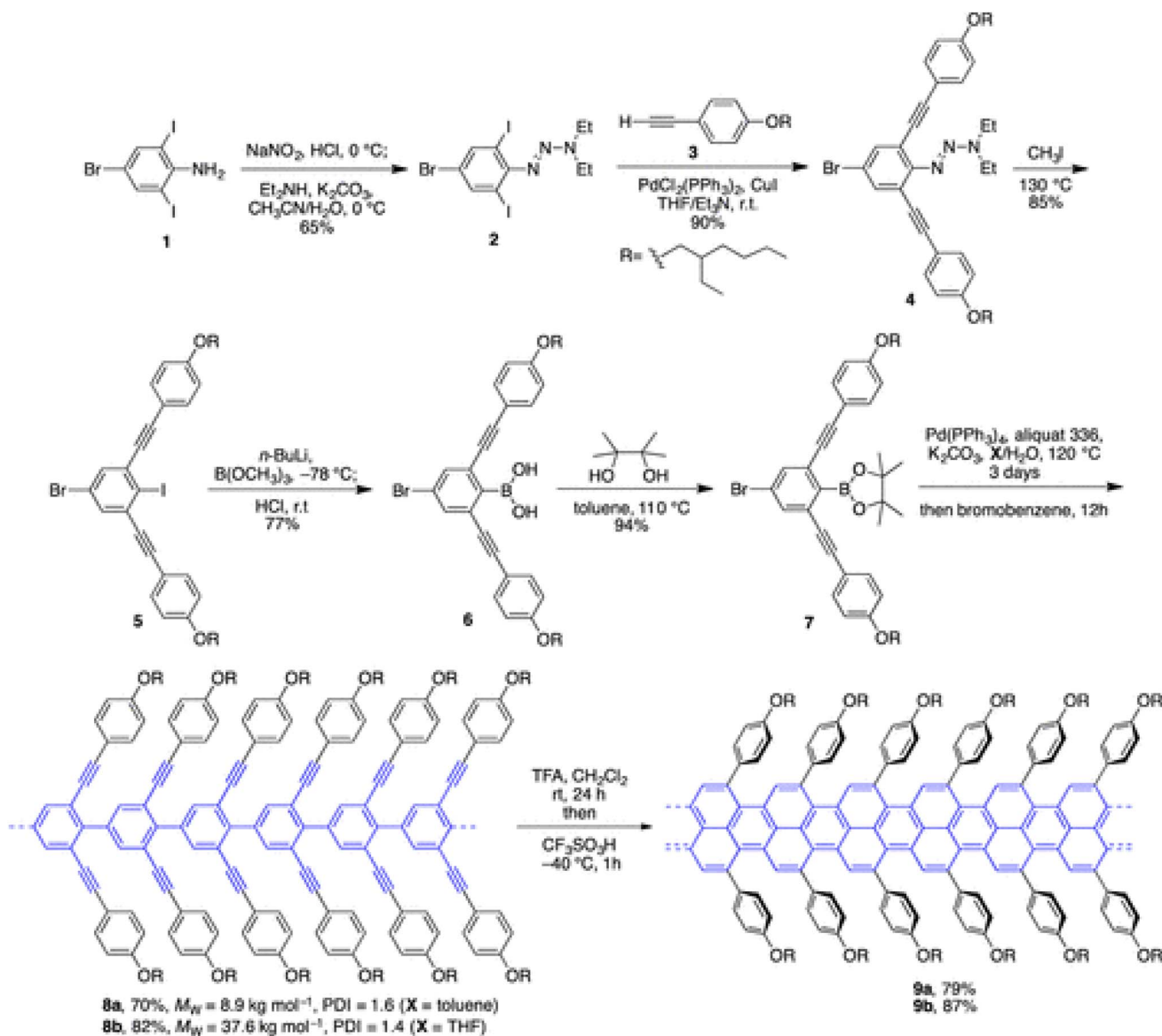
Fig. 11 Synthesis of PDAPP and its benzannulation to form GNR.[121]

resulted in laser-induced graphene formation within the upper 5 μm of the substrate, with a lateral resolution of approximately 12 μm, forming a pattern of around 60 μm in size as depicted in the images. In another study, using a CO_2 infrared laser scriber,[133] devised an alternative method for fabricating 3D porous graphene on PI in ambient settings. Using this novel method, modified PI (m-PI) was created by combining poly(-amic acid) (PAA) with N-methyl-2-pyrrolidone additions and then drying the mixture. When the m-PI was exposed to laser light, different compositions of LIG were formed. The thicknesses of the LIG produced ranged from 20 μm to 1 cm. The researchers then looked at how LIG formed on lignocellulose materials such as bread, potatoes, and wood. The results were good; when a defocused laser point of about 1 mm was employed to laser-seed in an inert or reducing environment, many wrinkles appeared in the LIG. Furthermore, this team

investigated the feasibility of scale-up manufacturing to meet the needs in practical applications, and they presented two solutions for the mass production of LIG.[133]

Kulyk's research team also created LIG on cellulosic materials by irradiating filter paper with a CO_2 laser.[134] The study explored how various factors like distance between substrates, scanning speed, and laser intensity impacted the result. Creating paper LIG involved two laser phases: the first, out-of-focus phase charred the cellulose, while the second, in-focus phase transformed the char into LIG. To prevent cellulose from becoming LIG prematurely, 6×6 mm² filter paper pieces, 290 μm thick, were treated with a fire retardant. Using a power of 1.1 W caused significant damage to the paper, while powers ranging from 600 to 800 mW were effectively utilized without harm. Different scanning speeds and defocusing distances were tested, resulting in samples retaining their fibre structure with

minimal visible flaws and maintaining high morphological integrity.[134] In another study,[135] created micron-scale LIG by irradiating a positive photoresist (PR), which is often used in commercial photolithography and is made of 15–25% Novolak resin. The scriber utilized for this process had a spatial resolution of around 10 μm and was made of a 10.6 μm CO$_2$ infrared laser. An acetone bath was used to dissolve the unsealed PR. To begin with, Si wafers were spin-coated with PR at 500–3000 rpm. Wafers were hard-baked at 120 °C for 45 minutes after spinning. As precursors, thin PR (3–8 μm) were used. A defocused laser beam repeatedly illuminates the same area because of the increase in spot size. To produce LIG in one pass, a defocus of 1.78 to 2.54 mm is needed. As the frequency of laser passes rises, the thickness of the defocused laser LIG varies. Initially, its growth is fueled by the development of gas impurities on the initial laser surface, yet it gradually diminishes as additional material is vaporized and graphene is generated through successive laser treatments. The sheet resistance fluctuates based on laser intensity, the number of treatments, and the deviation in focus, all contingent on the specific conditions during laser processing. Due to film degradation in the form of blistering or cracking, it has lower values at high power. Moreover, doing more passes enhances the sheet resistance.[135]

Researchers have also tried to use pulsed laser irradiation to ablate carbonaceous targets in liquid, vacuum, and gas environments to fabricate GBM.[136–138] For the first time, Qian's research group[137] detailed their findings on producing 2D graphene by employing pulsed laser exfoliation of HOPG with a pulsed neodymium-doped yttrium aluminum garnet (Nd:YAG) laser. They utilized a 532 nm laser with a pulse width of 7 ns, repeating at 1 Hz, and varying laser fluences from 0.8 to 20.0 J cm^{-2}. The substrate employed was a silicon wafer. The substrate was a silicon wafer. Different phases of carbon nanostructures, such as thin graphite films, few-layer graphene, and amorphous carbon, were created. In particular, GSs with dimensions of tens of micrometres, a thickness of a few nanometers, and a diameter of around 3.9 nm were produced. In like manner, as shown in Fig. 12, Nancy's work[139] served as an example of a unique laser-induced synthesis of silver nanoparticles (Ag NPs) that are attached to the GO layers using a single-step green approach known as pulsed laser ablation. Colloidal Ag–GO nanohybrid materials are created by producing Ag NPs from a bulk solid silver target ablated in an aqueous solution of GO using the second and third harmonic wavelengths (532 nm and 355 nm) of a Nd:YAG pulsed laser.

Russo, Hu[140] also reported a novel, green, scalable, and one-pot method for synthesizing graphene quantum dots and porous graphene by ablation of HOPG in water utilising a pulsed laser with a wavelength of 800 nm, a repetition rate of 1 kHz, a pulse duration of 35 fs, and a fluence of 20–30 J cm^2. For 20 minutes, the precursor was ablated continuously at a steady fluence. Porous graphene (quantum dots) of varying layer thicknesses, spanning from one layer to many sheets, were observed abundantly within the product generated post-ablation, looking like stacked layers floating atop the water–air interface of the resultant solutions. Their typical diameters were ≥100 but ≤200 nm, featuring a textured surface marked by folds attributed to the deposition process of the silicon substrate. Exhibiting a three-dimensional porous architecture, the layers contained pores ranging from 10 to 20 nm in size.[140] Generally, laser-induced graphene commonly has high thermal stability greater than 900 °C, admirable conductivity between 5–25 S cm^{-1}, and a high SSA of up to 340 m^2 g^{-1}.[141] This approach is better than CVD since it may be carried out in conditions where accurate regulation of pressure and the presence of ultra-pure gases are not necessary. In addition, by using roll-to-roll automation, it may be readily scaled up to produce graphene on a huge scale, offering tremendous commercialization prospects.

2.3 Applications of GBMs in gas adsorption

Air purification has become increasingly important because the pollution of air is linked to several health problems including respiratory diseases and premature deaths.[142,143] Chief among the pollutants that continue to be of concern are oxides of nitrogen, sulphur and carbon, due to their participation in the formation of smog and acid rain as well as their adverse effects on human health.[144,145] They are generally formed at high temperatures through an endothermic reaction in the gas phase.[146] In general, these dangerous gases and particles are released into the atmosphere from factories, automobiles, forest fires, open burning of insecticides, and even domestic and commercial goods. Carbon-based materials such as graphene have attracted significant attention as adsorbents over the years.[147] The large surface area and unique structure of graphene-based materials (GBMs) makes them useful as superior adsorbents for the removal of various pollutants from the environment.[148] The extreme hydrophobicity of graphene coupled with its high specific surface area gives it excellent
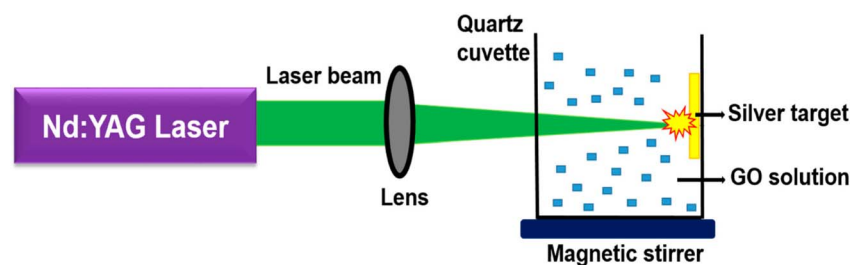

Fig. 12 The setup for producing colloidal Ag–GO nanohybrid graphene.[139]

properties for adsorbing hydrophobic organic compounds, thus making it an excellent choice as adsorbents in air purification.[149]

2.4 Adsorption and conversion of volatile organic compounds and PM$_{2.5}$ using GBMs

2.4.1. Adsorption of VOCs using GBMs. Volatile organic compounds (VOCs) represent toxic pollutants that emanate from several industrial sources including cleaning processes for silicon chips, plastic fabrication, paints, internal combustion engines, and the petroleum industry. Exposure to this group of compounds over a long period of time, even at very low concentrations, can pose adverse health effects comprising respiratory diseases, cancer, and kidney failure.[150,151] Owing to this, it becomes important to manage or remove VOCs from the environment. Various adsorbents have been investigated for the removal of VOCs including polymers, silica, zeolites, and activated carbon.[152] The efficiency of the adsorption process is predicated on the adsorbent's pore size distribution, specific surface area, and the chemical affinity between the VOC pollutants and the adsorbent.[153] Graphene represents a significant upgrade over the aforementioned adsorbents in terms of its high specific surface area and it is relatively easy to chemically modify graphene for the formation of active sites that allows the capture and/or removal of target pollutants.[154] A summary of studies that reported the various efficiencies of graphene-based materials in the adsorption of VOCs is presented in Table 1.

Graphene-based adsorbents were employed in a study to remove acetaldehyde and toluene gases. The study treated graphene oxide with KOH activation and microwave irradiation to form micro sized pores. The results of the study indicated that the graphene surface expanded, and its specific surface area increased when pristine graphene was heated to about 800 °C under KOH activation and then exposed to microwave radiation. Impressive maximum volume capacities of 3510 m^3 g^{-1} for toluene and 630 m^3 g^{-1} for acetaldehyde gas were demonstrated by the material. The exceptional removal efficiency of toluene (98%) in contrast to acetaldehyde (30%) gas was ascribed to the strong interactions that transpired between the toluene molecules and the pristine graphene surface.[156] In consonance with the literature, the adsorption of toluene on the graphene material is largely due to the non-covalent interaction occurring between the aromatic ring of toluene and the π electron-rich region in the basal plane of the graphene.[168,169]

In addition, adjusting several factors such as surface functional groups, humidity, boiling point, polarity, pore distribution, pore size, and specific surface area have been shown to enhance the chemisorption or physical adsorption performance of adsorbents.[170,171] A study investigated the use of mesoporous graphene powders produced by thermal expansion method as adsorbents in the removal of toluene and xylene.[162] The results of the study showed that the thermally expanded graphene powder (TEGP) exhibited relatively high adsorptive capability at each tested concentration of toluene and xylene. Despite the high specific surface area exhibited by TEGP, there were variations in its total adsorbed volume capacity of toluene and xylene, suggesting that the adsorption of the gas molecules is not only predicated on specific surface area. It is noteworthy to point out that the study reported 691 cm^3 g^{-1} and 191 cm^3 g^{-1} total adsorbed volume capacities for toluene and xylene, respectively. This significant variation was attributed to the relatively smaller molecular size of toluene which indicates

Table 1 Summary of studies that reported the various efficiencies of graphene-based materials (GBMs) in the adsorption of VOCs

GBMs	Volatile organic compound	Adsorption capacities	Removal efficiency (%)	Reference
ZIF-8/GO	Toluene	116 mg g^{-1}	—	155
rGO/KOH	Acetaldehyde	630 mm^3 g^{-1}	—	156
rGO	Toluene	454 mg g^{-1}	—	157
Graphene-PhAPTMS	Toluene	—	>95	158
Cu-BTC/GO	Toluene	183 mg g^{-1}	—	159
rGO/polypyrrole	Benzene	15.8 mmol g^{-1}	—	160
GO/ordered mesoporous carbon composite	Benzene	9.6 mmol g^{-1}	—	161
rGO MW/KOH	Toluene	3510 mm^3 g^{-1}	98	156
	Acetaldehyde	630 mm^3 g^{-1}	30	
Thermally expanded graphene powder	Toluene	691 cm^3 g^{-1}	92.7–98.3	162
	Xylene	191 cm^3 g^{-1}	96.7–98	
Few layered mesoporous graphene	Toluene	—	260 mg g^{-1}	163
Graphene/metal–organic composites	Benzene	—	72 cm^3 g^{-1}	164
rGO	Benzene	—	276.4 mg g^{-1}	149
	Toluene	—	304.4 mg g^{-1}	
Thermally exfoliated graphene oxide	Benzene, toluene, xylene	—	98 ± 2	165
Graphene	Benzene	8.8–158 mg g^{-1}	—	166
	Xylene	8.53–156 mg g^{-1}		
	n-Hexane	7.13–126 mg g^{-1}		
	Toluene	8.76–162 mg g^{-1}		
	Carbon tetrachloride	9.6–166 mg g^{-1}		
L-GO/polypropylene masks	Xylene	804 mg g^{-1}	98.9	167

more of the toluene gas would be adsorbed at any given volume.[162]

It has been suggested that the specific technique adopted in building graphene architectures is an influential factor for its hierarchical porosity and large specific surface area. Some of the widely adopted techniques have included activating the graphene material with various activating agents.[172–174] However, these activating agents cause the resulting activated graphene materials to exhibit extra hydrophilic sites and random porous architectures. To circumvent this, the chemical vapour deposition method stands out as a promising and attractive technique in the construction of graphene materials with mesoporous structures for the adsorption of VOCs.[175–177] Wang *et al.* (2019) employed a graphene material fabricated by the chemical vapour deposition method in the adsorption of toluene. The study showed that a three-dimensional architecture made of graphene layers was demonstrated using the as-prepared few-layered mesoporous graphene (FLMG). The remarkable adsorption capabilities of FLMG were a result of its distinctive architecture, especially when it comes to toluene at low concentrations (120 ppm). Strong π–π interactions and a large specific surface area (SSA) of 1990 $m^2 \, g^{-1}$ were important factors in this adsorption behaviour. Interestingly, even at a low heating temperature of 95 °C, a high desorption ratio of 92% ± 4% was achieved owing to interconnected mesopores that promote efficient desorption. These features allow FLMG to demonstrate reusability. Furthermore, FLMG is endowed with inherent thermostability and hydrophobicity *via* the chemical vapour deposition technique. FLMG maintained 80.1% ± 3.4% of its initial adsorption capability even at high humidity levels.[163]

Similarly, another study employed the use of the chemical vapour deposition method in synthesizing graphene and the activated graphene was used in the adsorption of benzene, toluene, and xylene.[178] The results of the study showed that the activation of the graphene material increased its surface area from 298 to 568 $m^2 \, g^{-1}$. In addition, the study reported that a significant quantity of benzene, toluene, and xylene was adsorbed from a typical gasoline vapour using the synthesized activated graphene, highlighting that hydrophobic interactions, π–π bonds, and electrostatic interactions are the effective forces responsible for the adsorption of these compounds.[149,178]

Graphene oxide has phenolic hydroxyl and epoxide groups on its basal plane and carboxylic groups on its edges. Reduced graphene oxide is generally produced by thermal annealing or chemical treatment which eliminates the functional groups present on the graphene oxide.[148] The reduced graphene oxide is preferred to graphene oxide due to its higher surface area, higher hydrophobicity, and lower oxygen content, all of which give it superior adsorption capability.[179] A facile and cost-effective method was adopted by Yu *et al.* (2018) to prepare reduced graphene oxide, which adopted for the adsorption of VOCs. According to the results of the adsorption experiment, reduced graphene oxide was able to adsorb more benzene and toluene than graphene oxide. At room temperature and normal pressure, reduced graphene oxide's breakthrough adsorption capacity was 304.4 $mg \, g^{-1}$ for toluene and 276.4 $mg \, g^{-1}$ for benzene, respectively.[149]

Recently, extensive research has been carried out to enhance the adsorption efficiency of carbon-based materials by modification using metal elements.[180–182] A density functional calculation study was conducted by Liu *et al.* (2019) to understand the adsorption mechanisms of pristine PG monolayer and Al-modified PG (Al-PG) monolayer in the removal of VOCs. The findings of the study showed that PG monolayers are excellent adsorbents for volatile organic compounds (VOCs). The adsorption energy of carbonyl-containing VOCs (CVOCs) is enhanced further after Al decoration, and it is nearly twice as high as that of CVOCs adsorption on PG monolayer. The electronic structure analysis (Mulliken charge distribution, electronic density distribution, and the density of state) revealed that the carbonyl group can attract the Al atom with the formation of a C–Al bond, which causes the connection of CVOCs and Al-PG substrate in the adsorption process and also greatly strengthens the adsorption of CVOCs.[183]

Despite the great application potential shown by porous carbon materials including graphene in the adsorption of VOCs, most of these porous materials exist in block or powder form and as such cannot be used in wearable personal protective applications. Polypropylene masks are more flexible and comfortable to wear than carbon materials, but they are unable to intercept small VOCs due to electrostatic interactions and visible fibre pores. Hence, a possible combination of carbon materials and polypropylene masks would result in a personal protective fabric with the ability to effectively absorb VOCs. This led Cheng *et al.* (2024) to create a novel method for carbonizing polypropylene mask surfaces by making use of graphene's superior laser responsiveness. To create a thick layer of graphene oxide, they applied an aqueous solution of the material to the mask's surface. Next, they used a more controllable 1064 nm near-infrared laser to irradiate the graphene oxide coating.[167] This novel double-layer fabric has two functions: it efficiently performs solar-powered desorption and recycling and recovers low-concentration VOCs from gas, achieving about 98.9% removal in just 30 seconds. The fabric's design makes use of easy-to-use and cost-effective coating and laser irradiation techniques. The hydrophilic porous channels created by laser-induced thermal degradation of graphene oxide coatings in ambient air are responsible for this fabric's exceptional adsorption capability. These channels help conjugated double bonds and hydrophilic groups interact with the benzene rings found in VOCs.[167]

From the foregoing, it suffices to say that the utilization of graphene composites, which involve combining graphene with other materials, significantly broadens their range of applications. In most cases, the removal efficiencies were well over 95%, suggesting that these materials are capable of removing the target VOCs. These composites are very useful in practical applications because they have additional characteristics, including chemical stability, mechanical strength, and flexibility. Novel strategies for solar-driven desorption and recycling improve the energy efficiency and sustainability of graphene-based adsorbents. This is in line with the increasing emphasis on eco-friendly technologies. Additionally, the creation of wearable and flexible adsorbent materials presents

intriguing new opportunities for personal protective equipment, particularly in environments where VOCs are present in high concentrations.

2.4.2. Adsorption of PM$_{2.5}$ using GBMs. The pollution of the environment by particulate matter has its attendant effects on public health and global air quality.[184,185] Based on particle size, it can be divided into PM$_{2.5}$ and PM$_{10}$, with the former describing particle sizes with aerodynamic diameter $\leq$2.5 μm and the latter describing particle sizes with aerodynamic diameter $\leq$10 μm.[186] PM$_{2.5}$ can easily enter the lungs and human bronchi, and consequently circulate through the blood owing to the ultrafine diameter.[187,188]

A large surface area is essential for any adsorption-based filter. If the surface area were greater, more particulate matter would be caught during the process of adsorption onto the filter surface. Broadly speaking, a two-dimensional (2-D) material is larger than a three-dimensional (3-D) material by nature in terms of surface area per weight. Most of the filters used currently are 3-D nanofibers or nanoparticles.[189] This informed the development of a 2-D material, reduced graphene oxide, in the design of a filter for the removal of PM$_{2.5}$.[189] According to the findings of the study, the filter's highly porous and void structure minimizes pressure loss while allowing air to flow through it quickly. Particulate matter (PM) can be effectively removed because there are enough sites for adsorption on the wide surface area. Interestingly, the quality factor of the filter is almost twice as high as the best-reported literature values. Additionally, dual filtering for both incoming room air and recirculated air is made possible by the foam built on both sides of the copper mesh. The filter's robustness is demonstrated by the fact that it still performs more than 99% PM reduction after five cleaning and reuse cycles. Its low power consumption, bi-directionality, scalability, and ease of manufacture make it a viable option for high-efficiency PM$_{2.5}$ removal filters.[189]

A relatively recent technique called electrospinning can be used to create ultrathin polymer and polymer composite fibres. A new and flexible technique for creating fibres made of spiderweb-like nanowebs that may be used for a range of applications is electrospinning.[190] Due to their huge surface area and great mechanical strength, electrospun fibres are able to collect both ultrafine particles and high-mass droplets. Additionally, because of the advantages of the reticular support structure and winding pore channels, electrospun fibres can be used to synchronously implement air flow and have the desirable capacity to tackle PM.[191] Dai *et al.* (2021) prepared a PAN/GO/PI nanofibrous membranes by incorporating graphene oxide and polyimide into a solution of polyacrylonitrile. When compared to pure PAN and PAN/GO nanofibrous membranes, the air filter made of PAN/GO/PI nanofibrous membranes was more successful at capturing PM$_{2.5}$ particles. The PAN/GO/PI nanofibrous membranes exhibit exceptional mechanical properties, superior thermal stability, reduced pressure drops, and great filtering efficiency. The interaction between PM$_{2.5}$ particles and PAN/GO/PI nanofibrous membranes, which have the ability to draw in and firmly adsorb PM$_{2.5}$ particles, is responsible for the high filtration efficiency (99.5%).[192]

Similarly, a filter based on rGO-functionalised PAN nanofibrous membrane was fabricated by electrospinning and used in the removal of PM$_{2.5}$.[193] Based on both hydrogen bonding and dipole–dipole interaction forces, the study showed that the rGO nanosheets scattered on/in the PAN NFM significantly increase the PM$_{2.5}$ capture sites on the uncross-linked nanofibers. Furthermore, because of the superior mechanical qualities of the rGO nanosheets, the tensile strength of the rGO-functionalized PAN NFM (0.48–1.25 MPa) is significantly higher than that of the pure PAN NFM (0.19 MPa). During air filtration, the composite NFM's increased tensile strength efficiently increases gas permeability. Thus, for resisting the airflow with a high gas velocity of 20 L min^{-1}, the ideal NFM containing 2.5 wt% rGO nanosheets demonstrated >99.9% PM$_{2.5}$ removal efficiency, 0.094 Pa^{-1} quality factor, and only 70 Pa pressure loss.[193]

Graphene aerogels areemerging super elasticity macroscopic and low-density porous materials with a wide range of uses. The development of a flexible approach for large-area, high-performance graphene aerogels at ambient conditions, which is essential for their practical applications, is still a difficulty.[194] Yan *et al.* (2019) developed a strategy to fabricate graphene aerogels under ambient conditions and this was used in the adsorption of PM$_{2.5}$. The results of the study showed that the as-formed aerogels are suited for pressure/strain sensors because of their super-elasticity (rapidly recoverable from 95% compression), low density of 3.6 mg cm^{-3}, and stable honeycomb-like coarse-pore structure. Additionally, aerogel shows strong recycling potential and better particulate matter adsorption efficiency (PM$_{2.5}$: 93.7%).[194]

Furthermore, most of the current research on air purification using graphene is widely focused on the mixing of graphene with other additives to obtain composite materials. However, Zou *et al.* (2019) prepared a graphene oxide membrane and used it in air purification. The efficiency of particulate matter (PM) removal as well as the effects of wind speed and pollutant concentration on a graphene oxide (GO) membrane were examined in the study. Notably, the GO membrane attained its maximum efficiency of 99.46% PM$_{2.5}$ removal at a wind speed of 0.1 m s^{-1}, with a minimum pressure drop of 7 Pa and a quality factor (QF) of 0.75 Pa^{-1}. The GO membrane exhibited prolonged adsorption efficiency. Furthermore, the removal effectiveness of the GO membrane was improved by larger import concentrations and lower wind velocities. The effective PM$_{2.5}$ capture by the GO membrane was verified by energy-dispersive X-ray spectroscopy (EDS) and scanning electron microscopy (SEM).[195]

The high efficiency of graphene-based materials in the adsorption of PM$_{2.5}$ has been demonstrated in this study. Nevertheless, it is imperative to ensure the high effectiveness of PM$_{2.5}$ filtration in addition to an ideal airflow with minimum pressure drop. Previous research has focused on methods to minimize pressure loss; nevertheless, more studies are needed to guarantee efficient air circulation in practical situations. There are still issues with the cost-effectiveness and scalability of graphene-based filters. Even though laboratory-scale research shows promising results, it is still unclear how large-scale manufacturing and commercial viability can be achieved.

2.5 Adsorption and conversion of nitrogen oxides using GBMs

NO_2 and NO are emissions of combustion processes occurring in internal combustion engines.[196] Hence, there is a need to ensure the preservation of air quality by developing efficient methods that can effectively remove nitrogen oxides.[197] Pristine graphene was used in a study for the adsorption of NO using the first-principle method. The adsorption process between molecular nitrogen monoxide (NO) and graphene, with adsorption energies ranging from -2.37 eV to -1.74 eV, was essentially physical, according to the findings of the study. A small number of electrons, with values between -0.007 e and -0.001 e, were moved from the NO molecule to the graphene surface during this process. Subsequent computations demonstrated that the graphene surface's B-site had the highest NO adsorption energy, followed by the T-site and the H-site. Analysis of the LUMO, HOMO, electron density difference, and Mulliken charge supported these findings. Generally, graphene was essential for adsorbing NO exhaust gas. Notably, the adsorption effect was especially beneficial when the B-site functioned as the adsorption site.[198]

Graphene was doped with transition metals (Cu, Ni, Co, and Fe) and it was investigated in the adsorption of NO, NO_2, and other gas molecules. The adsorption properties were calculated using a first-principle study.[199] The results of the DFT study indicated that among all the metal dopants, only Fe exhibited covalent bonding with graphene. The greater oxidation state of the Fe atom was attributed to be the likely cause of this phenomenon. Interestingly, in terms of charge transfer, the adsorption energy linked to transition metal doping is greater than that of pure graphene. Moreover, Fe exhibited the best adsorption energy, charge transfer, and intermolecular distances when transition metal atom doping is taken into account.[199] Furthermore, doping has been reported to enhance the electronic behaviour of semi-conductor materials.[200] Many kinds of dopants have been adopted to enhance and expand the applications of graphene.[201–203] The use of aluminum has been associated with the modification of electron density allocation around the doped atom and this has found applications for different purposes.[204–206] In a study, a nanostructure adsorbent, Al-modified graphene, was developed for the adsorption of N_2O and NO_2, with density functional theories.[207] The study showed that introducing aluminum (Al) doping to the graphene structure can significantly change the originally weak physisorption of gas molecules on pristine graphene into chemisorption. The electronic structure of graphene is altered by the presence of doped Al, which leads to strong adsorption of the gas species. Interestingly, Al-doped graphene (AlG) showed high adsorption of these gas molecules, but pristine graphene (PG) showed weak adsorption. The density of state analysis (Fig. 13) successfully confirmed this contrast.[207]

Moreover, tuning the thermoelectric, optical, electronic, mechanical, and structural properties of two-dimensional layered materials is widely influenced by native defects.[208–211] The presence of inactive surfaces on pristine graphene has led to low adsorption energies during the detection of several gas

molecules.[212,213] However, the chemisorption of gas molecules is facilitated by the presence of defects in graphene.[214] It has been suggested that the enhancement and induction of selectivity can be achieved by decorating graphene with nano-composites.[215,216] Ali and Tit (2019) carried out a study to investigate the adsorption of NO and NO_2 on ozone-treated graphene using density functional theory. The findings indicated that in addition to improving the selectivity of the sensor, ozone treatment of graphene requires more carbon vacancies in order to accommodate gas molecules. In agreement with experimental data, the findings showed that higher sensor response is a consequence of the chemisorption of NO_2 on graphene with mono-vacancy, compared to NO.[217]

Due to its exceptional structural qualities, such as its ultra-high specific surface area, and its electronic characteristics, such as its high electron mobility and low electrical noise, graphene, or monolayer graphite, has drawn a lot of interest in gas sensing.[218] Because surface adsorbates operate as electron donors or acceptors, they alter the local charge carrier density, which in turn affects the conductance of graphene sheets, which is the basis for several graphene-based sensors.[219] Because of its high surface area, strong chemical and thermal durability, high functionalization capability, and versatility in comparison to other nanostructure gas sensor systems, graphene is a good choice for high-sensitivity, label-free chemical sensors.[219,220]

Although pristine graphene by itself is not very good at sensing gases such as H_2O, NH_3, CO, NO_2, and NO,[221] scientists have discovered a useful method to improve its sensitivity and performance. This entails substitutional doping of graphene, which shows potential for creating even more sensitive sensors.[222] This informed the study undertaken by a group of researchers to investigate the comparative potential of pristine graphene and Ga-doped graphene in the adsorption of NO_2, NO and other gases using density functional theory.[223] The results of the study (Table 2) showed that there is little charge transfer because of the weak adsorption of gas molecules on pristine graphene. This is explained by the weak interaction between the gas molecules and graphene's π electrons. As opposed to pristine graphene, Ga-doped graphene showed a noticeably higher affinity for the studied gas molecules. Chemisorption on Ga-doped graphene was observed by analyzing the density of states (DOS) and electron density plots (Fig. 13). This process is characterized by comparatively high adsorption energies. Strong chemical bonds and a significant band gap are formed as a result of the interaction between the orbitals of gas molecules and the electron cloud. Due to prominent changes in the electronic structure and charge transfer between the gas molecule and Ga-doped graphene, NO_2 notably exhibited greater adsorption energies on Ga-doped graphene (Fig. 14).[223]

While a study showed that the adsorption of gas molecules including NO and NO_2 is significantly enhanced by decorating graphene oxide with lighter, cheaper, and more eco-friendly metals such as Al and Li,[224] another study investigated the doping of pristine graphene with Fe (FeG) and reported the high stability and increased adsorption of nitrogen oxides on FeG relative to pristine graphene,[225] and another study reported that
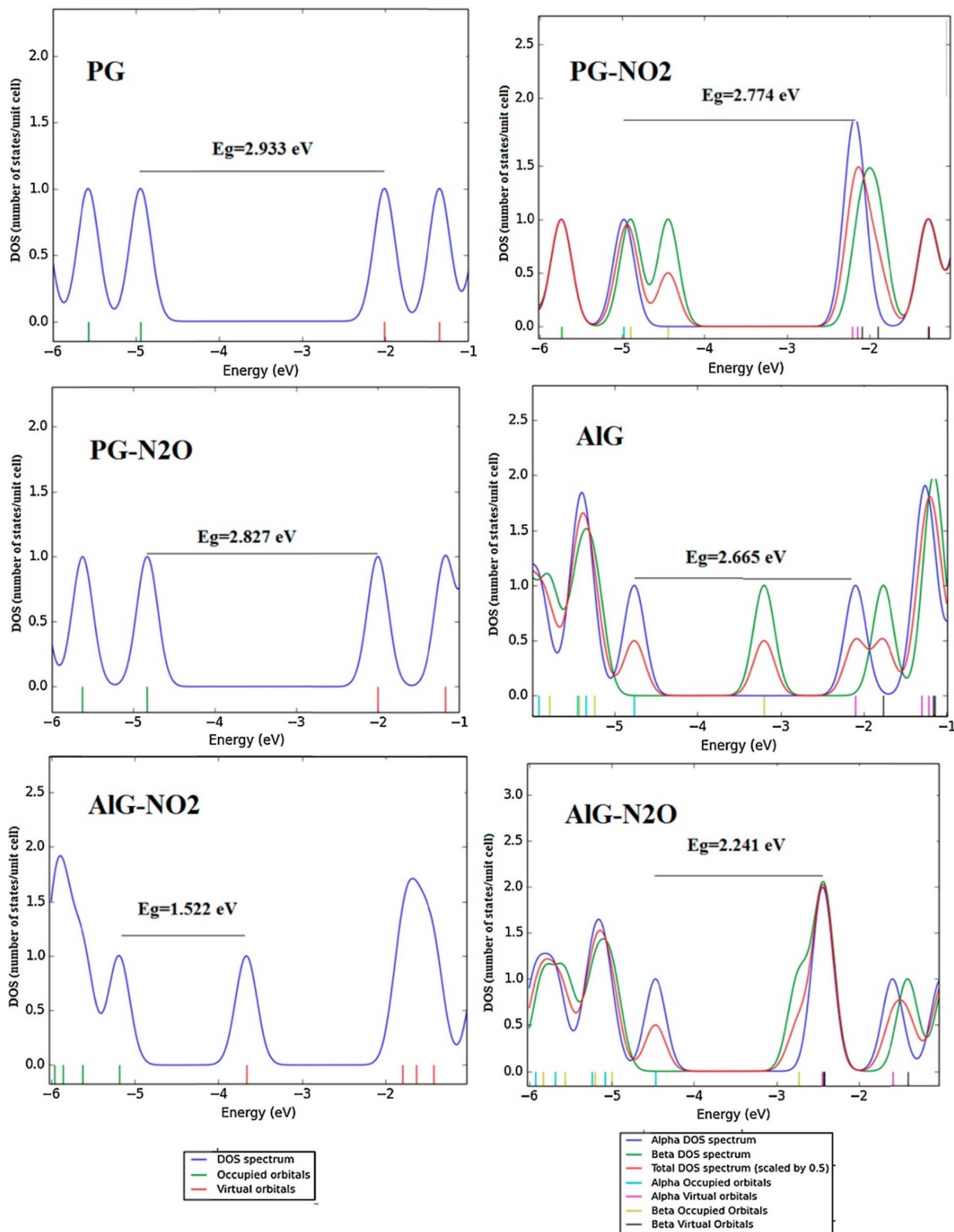
Fig. 13 The density of state for isolated PG, PG-NO$_2$, PG-N$_2$O, isolated AlG and the most stable configurations of AlG-NO$_2$ and AlG-N$_2$O.[207]

doubly doped defective graphene with boron, nitrogen and oxygen are more promising candidates for gas adsorption than pristine graphene although doubly doped defective graphene

with fluorine was reported to be unsuitable for gas adsorption owing to large structural deformation, high formation energy, and high recovery time despite its interaction with the gas

Table 2 Summary of the results showing the various adsorption energies of gas molecules on pristine and Ga-doped graphene[a][223]

Adsorbate	Pristine graphene			Ga-doped graphene		
	E_{ad}	Q	h	E_{ad}	Q	h
NO	−0.191	0.030	3.164	−0.779	−0.034	2.079
NO_2	−0.425	−0.199	2.841	−1.928	−0.239	1.957

[a] Where E_{ad} = adsorption energies, Q = Hirshfeld charge transfer, and h = adsorption height.

molecules in high adsorption energies,[226] the recurring theme in all of these studies is that doping significantly improves the adsorptive properties of graphene based materials towards gas molecules and this is consistent with many other studies in the literature.[227,228]

The adsorption of various gas molecules, including NO and NO_2, onto pristine graphene is characterized by weak physisorption. This phenomenon primarily arises from the relatively weak interaction between the gas molecules and the π electrons of graphene. Consequently, minimal charge transfer occurs, leading to low adsorption energies and corresponding adsorption heights. As highlighted, defect engineering and doping are pivotal in improving the adsorptive capabilities of materials. Nevertheless, it is important to learn more about the durability and resilience of these modified materials to make sure they are practically feasible. For practical applications, longevity and resistance to environmental degradation are equally essential. Getting graphene-based materials onto the market for gas adsorption will require overcoming the tremendous obstacle of scaling up manufacturing while maintaining consistent quality and performance. Material integrity must be balanced with mass production.

2.6 GBMs for adsorption and conversion of sulphur oxide

Sulfur oxides (SO_x) are major pollutants that are emitted from industrial processes such as fossil fuel combustion, metal smelting, and chemical manufacturing. The two primary pollutants in SO_x are sulfur dioxide (SO_2) and sulfur trioxide (SO_3). These pollutants contribute to acid rain, smog formation, respiratory problems, and environmental degradation. To mitigate their environmental impact, it is promising to convert SO_x into less harmful or valuable products. Graphene-based materials are renowned for their unique properties and are emerging as versatile platforms for catalyzing the conversion of SO_x. This article explores recent advancements and research endeavours in utilizing GBMs for the conversion of SO_x, highlighting their potential in sustainable air pollution control.

Pan and his colleagues synthesized HKUST-1, a widely utilized metallic organic framework (MOF), which several researchers have reported to be very reactive for the adsorption of toxic gases.[229] Despite its high reactivity, it has a major drawback of instability under humid conditions due to the interaction of water molecules with the unsaturated CU-site present on the surface of the HKUST-1 MOF. To overcome this drawback, HKUST-1 was modified with graphene oxide (GO) using hydrothermal methods. The result proved that 200 mg HKUST-1@1.2% GO synthesized hydrothermally performed excellently for the adsorption of SO_2 at 120 min, with an adsorption capacity of 72.49 mmol g^{-1}. HKUST-1@1.2% GO proved to be sustainable and stable, with the ability to absorb SO_2 over five cycles with only a 0.8% adsorption efficiency decrease observed.

In another study, SO_2 was adsorped on intrinsic graphene (IG), Ni-doped graphene (NiG) and Pd-doped graphene (PdG), respectively. It was theoretically studied based on the first principle of density functional theory. It was reported that there was a strong chemisorption between the contact surface with the E_{ads} of SO_2 molecules absorbed on NiG and PdG being −4.213 eV and −5.779 eV. the result also proved that the adsorption of SO_2 on IG was significantly improved due to the doping with Ni and Pd.[230] Interestingly another study by Karami and his colleagues reported the use of Beryllium-Oxide (BeO), Zinc-Oxide (ZnO), and Ni-decorated graphene applying the DFT first-principles study. The results also showed that the SO_2 molecules were chemisorbed on Ni-decorated graphene sheets with an adsorption energy of −2.297 eV as compared to the BeO and ZnO sheets which had physical adsorption.[231] Luo and his colleagues[232] conducted a study on the adsorption of SO_2 on graphene (G), N-doped graphene (N-G), Ti-doped graphene (Ti-G), and N–Ti co-doped graphene (N–Ti-G). They used DFT simulation and found that SO_2 molecules were adsorbed through physisorption on N-G and chemisorption on Ti-G and N–Ti-G. The study reported that N–Ti-G was the best material for SO_2 adsorption with the lowest adsorption energy −2.836 eV and excellent charge transfer $0.735e$ moved from N–Ti-G to SO_2, making it ideal for selecting and removing SO_2 (Luo et al., 2022).

The investigation of adsorption and oxidation of SO_2 on graphene oxides (GOs) GP, HO-GP, O-GP, and HO-OGP proved
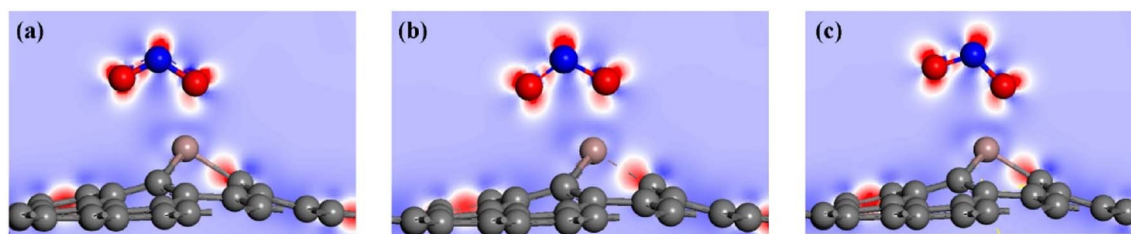

Fig. 14 Electronic deformation density for NO_2 molecule on Ga-doped graphene under an electric field of (a) 1 V per Angstrom, (b) 0 V per Angstrom and (c) −1 V per Angstrom.[223]
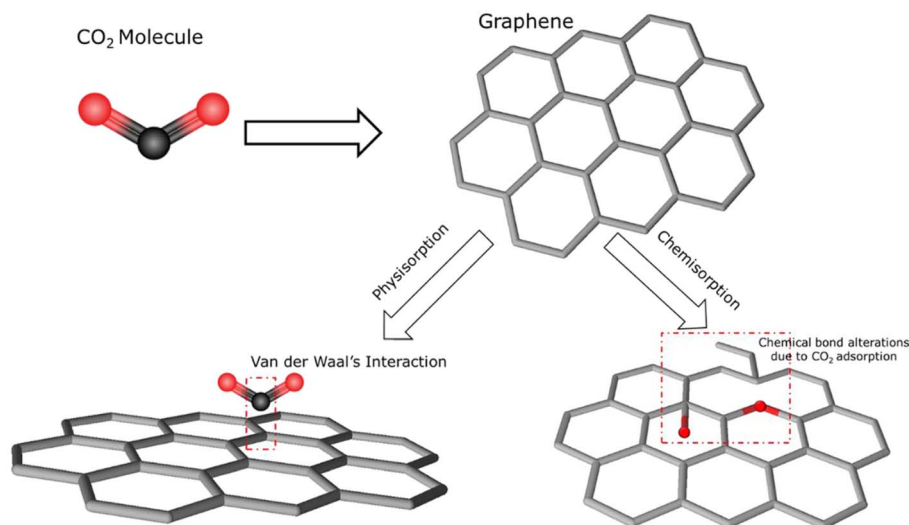
Fig. 15 Physisorption and chemisorption modes of graphene for CO_2 adsorption.

to be efficient and provided valuable insights into the mechanism. The study revealed that hydroxyl groups on the surface of GO enhance the adsorption of SO_2 through H-bonding interactions and reduce the reaction barrier for its oxidation to SO_3 due to its bifunctionality. The material's performance was reported as GP, HO-GP, O-GP, and HO-OGP, respectively.[233] Another researcher explored four graphene structures including pristine graphene (PG) vacancy-defected graphene (VG), Ti-doped graphene (Ti-G), and Ti-doped graphene with vacancies (Ti-VG) explored for the adsorption of SO_2 using the DFT first-principle calculations. It was reported that PG and vacancy defects formed very weak physical adsorption of SO_2. Upon doping with Ti, the adsorption energy and charge density of the adsorption system improved and also promoted chemisorption.[234]

DFT first principle calculations were utilized to investigate the efficacy of Co-doped (CoG), Ti-doped (IG-Ti), and Co–Ti co-doped (CoG-Ti) graphene on SO_2 adsorption.[235] CoG-Ti had the optimum performance for SO_2 adsorption with its adsorption energy as $-4.635\ E_v$. It was reported that the performance of the doped graphene was better than that of the intrinsic graphene (IG) for SO_2 adsorption based on the results of the analysis of the materials' structures and electronic properties at different adsorption sites.

2.7 CO_2 capture using GBMs

A significant portion of the energy systems in use today are based on fossil fuels, which continuously generate CO_2, the primary driver of global climate change.[236] Research and development on carbon cycle solutions and emissions management are crucial to mitigating the effects of global warming. By achieving zero carbon emissions, carbon dioxide (CO_2) capture and storage can slow down the acceleration of climate change.[237] To address this challenge, graphene may be used as a molecular sieve to capture CO_2 by its inherent holes and defects.[238–240] While the yield of graphene made from

naturally occurring carbon precursors is limited, the cost requirements of GBMs made from industrially derived raw materials are very high. Reduced graphene oxide (RGO) and other composites of graphene are effective alternatives for CO_2 capture material besides pure graphene.[241–243] Moreover, functionalizing GBMs is a standard procedure to increase their capacity for CO_2 adsorption.

The sorbent material's chemical and physical properties determine the mechanism of CO_2 adsorption. GBM has been shown to be able to absorb CO_2 through both chemisorption and physisorption.[244] GBMs have a large surface area, which provides a large number of CO_2 adsorption sites. Physisorption of CO_2 is driven by van der Waals interaction, which involves weak bonds between molecules of similar sizes without a net charge and does not require the formation of chemical bonds, the sharing of electrons, or modifications to the chemical structures of interacting molecules.[245,246] The physisorption mechanism is driven by weak van der Waals interactions between the graphene surface and the CO_2 molecules (Fig. 15).

The efficacy of GBM in capturing CO_2 is influenced by various factors such as temperature, pressure, and the presence of other gases.[247] Higher temperatures lead to a decrease in van der Waals interactions between CO_2 molecules and the graphene surface, resulting in reduced adsorption capacity. This reduction is indicative of an exothermic nature of physisorption. The binding energy for physisorption typically ranges from 20 to 40 kJ mol^{-1}.[248] Lower pressures diminish graphene's adsorption ability due to fewer CO_2 molecules available for adsorption. Gases like N_2, O_2, CO, and CH_4, which share similar kinetic properties with CO_2, can compete for adsorption sites, affecting graphene's selectivity for CO_2.[249] Additionally, moisture in the gas stream decreases graphene's adsorption capacity by blocking adsorption sites and hindering CO_2 facilitation on the adsorbent surface.

The CO_2 adsorption performance and surface area of GBMs are compared in Table 3. It is quite instructive to note there is

Table 3 Adsorption capacities of graphene-based materials (GBMs) for CO_2 capture

GBMs	Surface area ($m^2 g^{-1}$)	CO_2 adsorption capacities (mmol g^{-1})	Reference
Graphite nanofibers	567	59.2 mg g^{-1}	252
Graphene	443	2.16	253
GO/TiO$_2$	99.536	1.88	254
GO/ZnO	236	44.8 cm^3 g^{-1}	255
meta-Phenylenediamine-GO	44.33	0.61, 0.74, and 0.91 for GO-PEHA, GO-TETA, and GO-MPD	256
Triethylenetetramine-GO	14.40		
Pentaethylenehexamine-GO	9.39		
EDA-GO cryogels	167.66	1.18	257
Chitosan-GO cryogels	33.32	0.257	258
Urea-KOH-GO	1032	2.40	259
CO_2-activated graphene	2518	4.06	251
NaOH-activated graphene	843	1.74	
3D crumpled graphene	1316	2.45	260
Monolithic rGO aerogel	1622	6.31	250
GO/MOF-200	3359	1.34	261
GO/Cu-MOF	1015–1820	2.50–9.05	262 and 263
UV-irradiated GO/Cu$_3$(BTC)$_2$	1097–1324	2.53–5.14	264
GO/UiO-66	1184	3.37	265
RGO/Polymer	110	3.56–3.85	266
GO/Polyaniline	<5	1.31	267
GO/MgO	12	2.79–3.34	268
RGO/PMMT	50.77	0.49	269
Graphene sheets	484	2.894	260

a positive correlation between the specific surface area of the GBMs and adsorption capacities. Furthermore, surface modification involving amine-functionalization, formation of aerogels, doping with MOFs, and activation of GBMs using CO_2 and NaOH/KOH have successfully demonstrated the potential to enhance CO_2 adsorption of GBMs. Following the works carried out separately by Yun *et al.* (2016)[250] and Xia *et al.* (2021),[251] an amalgamation of both methods that will involve CO_2 activation of monolithic RGO aerogel may be worth pursuing for the future advancement of CO_2 capture by GBMs. Furthermore, it is noteworthy to mention that most research so far focuses on creating adsorbents with increased adsorption capacity and reduced regeneration energy consumption. However, for engineering applications and real-world applications, research on practical aspects and adsorption techniques is also required, particularly for high CO_2 sources, such as flue gas and syngas.

3 Limitations of current research achievements

Graphene-based nanomaterials have been notable for various scientific and industrial interests in terms of gas adsorption and air pollution. However, certain limitations occur with translating these breakthroughs from laboratory experiments to practical implementation. These weaknesses appear on all levels, *i.e.* technical, environmental and economic levels and they do indeed hinder a seamless integration of graphene-based products in the mainstream market. One of the biggest challenges is the challenge of large-scale production of graphene and its derivatives, especially graphene oxide and reduced graphene oxide. Although such materials have excellent adsorption

in the laboratory settings, large-scale simulations that extrapolate this to an industrial scale have not been able to replicate it. The present production processes are not only economically demanding in terms of cost, energy and time, but they are usually characterized by degraded structural resilience or product discontinuity. This limits their commercial applicability, particularly in applications where lots of utilization needs and constant consistent performance are essential.

The other complex factor is the surface functionalization of the materials. The adsorptive property and selectivity of graphene can be improved through functionalization of the surfaces that are usually attained in processes where functional groups are introduced to the graphene. Although this is to the advantage of performance, technically it is difficult to deposit uniform and rigid functionalization, which does not have dramatic implications on properties of interest, *e.g.*, conductivity or surface area. Besides, the use of chemicals which are toxic and production of hazardous by-products that arise during the process of functionalization present some reservations in the minds of the people regarding safety and effect on the environment. On the other hand, adsorbents composed of graphene are prone to be destroyed in high moisture or at areas where chemical activities are taking place. When chemicals are exposed to wet or reactive gases and are allowed to agglomerate on the surface or structural collapse occurs, surface oxidation, surface agglomeration and structural collapse may occur and the resultant effect would require the materials to no longer be effective. This weakness does not make them suitable in the ambient air or industrial gas treatment units where stability is of utmost essence.

Also, there is the selectivity of the gases that makes the application of the graphene nanomaterials more difficult. On one hand, they have a large surface area and tunable chemistry and have been seen to be promising when utilised as a selective adsorbent. It turns out, however, when trying to apply these materials practically, that they are quite bad at the ability to distinguish between similar gas molecules, particularly in high high-complexity mixture. This is a generality that renders them of little value in life circumstances when more than a single pollutant could exist and require remediation with highly detailed action plans.

Finally, long-term application still faces significant challenges when it comes to regeneration and reusability. To ensure the economic viability as well as the operative feasibility of the graphene-based adsorbents, the adsorbents cannot only be deemed to guarantee high single-cycle performance, but they must also be able to exhibit high performance even after a number of adsorption–desorption cycles.

4 Prospects of GBMs for air clean-up and future research directions

Considering the extensive coverage of the GBMs in the preceding sections, it is very clear that adsorption-based gas separation holds great potential for future air purification applications. Nonetheless, it is also evident that notable advancements in the state of the art are required in various directions, that may require multidisciplinary strategy. To begin with, choosing the right sorbent is an essential step in gas adsorption systems and the synthesis of novel GBMs with improved adsorption capacities through eco-friendly and readily scalable synthesis pathways remains the primary challenge. Significant technological and cost benefits could result from an adsorption-based approach that uses economical and efficient GBMs. In particular, the physicochemical properties of GBMs should be controllable at the molecular level because of the potential correlation between structure/function relationships and gas adsorption capacity.

Newly synthesized GBMs meant for industrial use needs to show their effectiveness in different gas–solid contact systems (like fixed, fluidized, moving, or rotating beds) and in particular technological regeneration configurations (like pressure, temperature, electricity, or combined cycles). This evaluation is crucial because it finally establishes the economic viability of a technology for gas extraction. The full potential of GBMs can only be realized by selecting the ideal gas–solid reactor configuration and regeneration mode, with the goal of minimizing operating and capital costs and expediting the commercial deployment of GBM-aided adsorption technology. Indeed, it is clear that the nature of gas–solid contacting system and regeneration technique has a significant impact on the capture performance in terms of gas recovery, purity, and productivity, as well as the energy requirement. Therefore, it is germane that new computational and characterization techniques must be developed, in tandem with experimental research for further development of the most efficient systems. Furthermore,

computational techniques may also prove to be an extremely effective means of conducting rapid, extensive screening of novel materials and forecasting their properties. This advanced tool may also shed light on the dynamic conditions for the most promising GBMs for more real-world multi-component mixtures.

Different adsorption-based gas separation techniques using GBMs, reactor configurations, and regeneration modes have all been demonstrated at various scales. However, adequate techno-economic and life cycle assessment (LCA) studies are still missing, which would give a clear estimate of the cost of adapting GBMs in current plants, as well as the real energy costs brought on by this capture technology. Therefore, before GBM-based gas capture processes are implemented in actual plants, all the aforementioned factors and key points need to be comprehensively addressed.

The following are some performance metrics and potential research directions in gas capture with GBMs:

• Simplifying GBM synthesis will lower production costs, expedite preparation, and make it easier to analyze parameters influencing adsorbent properties. Investigate current synthesis techniques to find ideal circumstances, GBM-specific factors, and novel material architectures for improved gas absorption. Improve innovative synthesis techniques that make use of inexpensive chemicals and raw materials to drastically reduce manufacturing costs (e.g., waste biomass, industrial wastes).

• GBMs with high mesoporosity, microporosity, and specific surface area are prioritized to enhance gas adsorption capacity and kinetics. There is a need to select the most appropriate GBM for a certain industrial application while taking the synthesis method, material costs, manufacturing procedure, life cycle assessment, and modification techniques into account. It is necessary to increase GBMs' robustness in dealing with moisture. Hence, research on how contaminants and water vapor affect gas absorption is crucial for maximizing removal effectiveness.

• Creation of general protocols for gas capture that take into account textural features, performance standards, application types, and appropriate process condition ranges (temperature, pressure, gas concentration, desired gas purity). Techno-economic analysis should be utilized to analyze promising GBMs for industrial use, providing details on costs associated with stability, scalability, and technological variants, as well as GBM-specific parameters.

5 Conclusion

This review provides an extensive synthesis of the new studies on the usage of graphene-based nanomaterials (GBMs) in gas adsorption applications, focusing on the prevention of air pollutants, especially greenhouse gases such as CO_2 and volatile organic compounds (VOC). Unlike other studies, which focus mostly on graphene synthesis or sensor equipment, this review compares and contrasts in a critical manner the structural adjustment, composite assembly, as well as surface functionalization, that improve the adsorption performance, selectivity and recycling of GBMs in environmental compartments. This

gives an excellent framework upon which innovation at the lab scale can be converted to viable real-world solutions. It is worth noting that the review deliberately avoids the sensor-related discussions to increase the emphasis on the adsorption mechanisms as an area that is not often explored in more general surveys. Generally, the study can be described as a practical guide but a prospective tool for researchers who wish to establish ways to use graphene in order to remedy the maladies of environmental pollution. There is the need to promote the use of ecologically safe solvents and environmentally friendly synthesis techniques for GBMs to reduce energy use and environmental impact. In line with waste valorization and the circular economy concepts, natural resources, renewable biomass, and industrial waste should be explored as raw materials to synthesize gas capture materials. The main concern of climate scientists and environmentalists today is mitigating the effects of climate change that have resulted from more than a century of continuous and widespread greenhouse gas emissions. Thus, identifying and developing highly selective GBMs as well as adaptable methods for industry-based gas capture will be essential to reducing greenhouse gas emissions and keeping the planet safe.

Author contributions

OTO and AAB conceived and designed the study. DTA, AAB and OTO wrote the main manuscript draft. All the authors proofread and reviewed the manuscript.

Conflicts of interest

The authors declare that they have no competing interests.

Data availability

No primary research results, software or code have been included, and no new data was generated or analysed as part of this review.

Acknowledgements

References

1 I. Manisalidis, E. Stavropoulou, A. Stavropoulos and E. Bezirtzoglou, *Front. Public Health*, 2020, **8**, 14.

2 S. Maji, S. Ahmed, M. Kaur-Sidhu, S. Mor and K. Ravindra, *Air Soil. Water Res.*, 2023, **16**, 11786221231154659.

3 V. Cukic, V. Lovre, D. Dragisic and A. Ustamujic, *Mater. Sociomed.*, 2012, **24**, 100–105.

4 M. Sompornrattanaphan, T. Thongngarm, P. Ratanawatkul, C. Wongsa and J. J. Swigris, *Asian Pac. J. Allergy Immunol.*, 2020, **38**, 19–28.

5 V. V. Tran, D. Park and Y. C. Lee, *Int. J. Environ. Res. Public Health*, 2020, **17**(8), 2927.

6 H. C. Loh, I. Looi, A. S. H. Ch'ng, K. W. Goh, L. C. Ming and K. H. Ang, *J. Geo*, 2022, **87**, 4425–4437.

7 S. Barua and S. D. Nath, *J. Clean. Prod.*, 2021, **298**, 126755.

8 J. N. B. Bell, S. A. Power, N. Jarraud, M. Agrawal and C. Davies, *Int. J. Sustain. Dev. World Ecol.*, 2011, **18**, 226–235.

9 Z. Rafie-Rad, T. Raza, N. S. Eash, M. Moradi-Khajevand and M. Moradkhani, in *Health and Environmental Effects of Ambient Air Pollution*, Elsevier, 2024, pp. 71–90.

10 F. P. Perera, *Environ. Health Perspect.*, 2017, **125**(2), 141–148.

11 W. Fan, Q. Xin, Y. Dai, Y. Chen, S. Liu, X. Zhang, Y. Yang and X. Gao, *Sep. Purif. Technol.*, 2025, **353**, 128394.

12 J. Li, L. Liang, B. Lyu, Y. S. Cai, Y. Zuo, J. Su and Z. Tong, *Environ. Pollut.*, 2023, **338**, 122665.

13 S. S. Shetty, D. D, H. S, S. Sonkusare, P. B. Naik, N. S. Kumari and H. Madhyastha, *Heliyon*, 2023, **9**, e19496.

14 A.-M. O. Mohamed, M. A. Maraqa, F. M. Howari and E. K. Paleologos, in *Pollution Assessment for Sustainable Practices in Applied Sciences and Engineering*, ed. A.-M. O. Mohamed, E. K. Paleologos and F. M. Howari, Butterworth-Heinemann, 2021, pp. 491–554, DOI: 10.1016/B978-0-12-809582-9.00009-8.

15 V. Kumar, N. Sharma, P. Sharma, R. Pasrija, K. Kaur, M. Umesh and B. Thazeem, *Toxicol. Appl. Pharmacol.*, 2023, **474**, 116623.

16 L. Zhang, C. Ou, D. Magana-Arachchi, M. Vithanage, K. S. Vanka, T. Palanisami, K. Masakorala, H. Wijesekara, Y. Yan, N. Bolan and M. B. Kirkham, *Int. J. Environ. Res. Public Health*, 2021, **18**(21), 11055.

17 S. Baldacci, S. Maio, S. Cerrai, G. Sarno, N. Baïz, M. Simoni, I. Annesi-Maesano and G. Viegi, *Respir. Med.*, 2015, **109**, 1089–1104.

18 M. C. Maciag and W. Phipatanakul, *Ann. Allergy Asthma Immunol.*, 2022, **128**, 652–658.

19 V. Singh, D. Joung, L. Zhai, S. Das, S. I. Khondaker and S. Seal, *Prog. Mater. Sci.*, 2011, **56**, 1178–1271.

20 C. S. Yadav, I. Azad, A. R. Khan and P. Singh, in *Biosensors Based on Graphene, Graphene Oxide and Graphynes for Early Detection of Cancer*, CRC Press, 2025, pp. 1–23.

21 K. Cao, X. Ge, S. Li, Z. Tian, S. Cui, G. Guo, L. Yang, X. Li, Y. Wang and S. Bai, *RSC Adv.*, 2025, **15**, 17089–17101.

22 T. E. Thompson, E. R. Falardeau and L. R. Hanlon, *Carbon*, 1977, **15**, 39–43.

23 H. Fuzellier, J. Melin and A. Herold, *Carbon*, 1977, **15**, 45–46.

24 A. R. Ubbelohde and F. A. Lewis, *Graphite and its Crystal Compounds*, Clarendon Press, 1960.

25 O. A. Shenderova, V. V. Zhirnov and D. W. Brenner, *Crit. Rev. Solid State Mater. Sci.*, 2002, **27**, 227–356.

26 S. Stankovich, D. A. Dikin, R. D. Piner, K. A. Kohlhaas, A. Kleinhammes, Y. Jia, Y. Wu, S. T. Nguyen and R. S. Ruoff, *Carbon*, 2007, **45**, 1558–1565.

27 L. Niu, Q. Zhang, R. Zhang, D. Wang, G. Wen and L.-C. Qin, *Colloids Surf., A*, 2024, **691**, 133877.

28 G. Kubheka, A. O. Adeola and P. B. C. Forbes, *RSC Adv.*, 2022, **12**, 23922–23936.

29 F. Zhang, K. Yang, G. Liu, Y. Chen, M. Wang, S. Li and R. Li, *Composites, Part A*, 2022, **160**, 107051.

30 R. Kumar, S. Sahoo, E. Joanni, R. K. Singh, R. M. Yadav, R. K. Verma, D. P. Singh, W. K. Tan, A. Perez del Pino and S. A. Moshkalev, *Nano Res.*, 2019, **12**, 2655–2694.

31 R. Ma, Y. Zhou, H. Bi, M. Yang, J. Wang, Q. Liu and F. Huang, *Prog. Mater. Sci.*, 2020, **113**, 100665.

32 S. S. Emmanuel, A. A. Adesibikan, O. D. Saliu and E. A. Opatola, *Plant Nano Biol.*, 2023, **3**, 100024.

33 A. O. Adeola, M. P. Duarte and R. Naccache, *Front. Carbon.*, 2023, **2**, 1220021.

34 K. S. Novoselov, A. K. Geim, S. V. Morozov, D.-e. Jiang, Y. Zhang, S. V. Dubonos, I. V. Grigorieva and A. A. Firsov, *Science*, 2004, **306**, 666–669.

35 W.-W. Liu, S.-P. Chai, A. R. Mohamed and U. Hashim, *J. Ind. Eng. Chem.*, 2014, **20**, 1171–1185.

36 B. Jayasena, C. Reddy and S. Subbiah, *Nanotechnology*, 2013, **24**, 205301.

37 Y. Hernandez, V. Nicolosi, M. Lotya, F. M. Blighe, Z. Sun, S. De, I. T. McGovern, B. Holland, M. Byrne and Y. K. Gun'Ko, *Nat. Nanotechnol.*, 2008, **3**, 563–568.

38 A. A. Moosa and M. S. Abed, *Turk. J. Chem.*, 2021, **45**, 493–519.

39 G. Zhao, T. Wen, C. Chen and X. Wang, *RSC Adv.*, 2012, **2**, 9286–9303.

40 A. O'Neill, U. Khan, P. N. Nirmalraj, J. Boland and J. N. Coleman, *J. Phys. Chem. C*, 2011, **115**, 5422–5428.

41 N. Kumar, R. Salehiyan, V. Chauke, O. J. Botlhoko, K. Setshedi, M. Scriba, M. Masukume and S. S. Ray, *FlatChem*, 2021, **27**, 100224.

42 A. A. Bayode, D. M. dos Santos, M. O. Omorogie, O. D. Olukanni, R. Moodley, O. Bodede, F. O. Agunbiade, A. Taubert, A. S. S. de Camargo, H. Eckert, E. M. Vieira and E. I. Unuabonah, *J. Water Proc. Eng.*, 2021, **40**, 101865.

43 A. A. Bayode, E. M. Vieira, R. Moodley, S. Akpotu, A. S. S. de Camargo, D. Fatta-Kassinos and E. I. Unuabonah, *Chem. Eng. J.*, 2021, **420**, 127668.

44 D. R. Lide, *CRC Handbook of Chemistry and Physics*, CRC press, 2004.

45 J. Xu, D. K. Dang, V. T. Tran, X. Liu, J. S. Chung, S. H. Hur, W. M. Choi, E. J. Kim and P. A. Kohl, *J. Colloid Interface Sci.*, 2014, **418**, 37–42.

46 M. Yi and Z. Shen, *J. Mater. Chem. A*, 2015, **3**, 11700–11715.

47 Y. Hernandez, V. Nicolosi, M. Lotya, F. M. Blighe, Z. Sun, S. De, I. T. McGovern, B. Holland, M. Byrne and Y. K. Gun'Ko, *Nat. Nanotechnol.*, 2008, **3**, 563–568.

48 X. J. Lee, B. Y. Z. Hiew, K. C. Lai, L. Y. Lee, S. Gan, S. Thangalazhy-Gopakumar and S. Rigby, *J. Taiwan Inst. Chem. Eng.*, 2019, **98**, 163–180.

49 A. Saravanan, P. S. Kumar, S. Srinivasan, S. Jeevanantham, M. Vishnu, K. V. Amith, R. Sruthi, R. Saravanan and D.-V. N. Vo, *Chemosphere*, 2022, **298**, 134284.

50 H. Aghamohammadi, R. Eslami-Farsani, M. Torabian and N. Amousa, *Synth. Met.*, 2020, **269**, 116549.

51 P. Yu, S. E. Lowe, G. P. Simon and Y. L. Zhong, *Curr. Opin. Colloid Interface Sci.*, 2015, **20**, 329–338.

52 K. Parvez, R. Li, S. R. Puniredd, Y. Hernandez, F. Hinkel, S. Wang, X. Feng and K. Mullen, *ACS Nano*, 2013, **7**, 3598–3606.

53 H. Jiangbo and A. Ramadan, *J. Mater. Chem.*, 2011, **21**, 15009–15014.

54 S. Y. Sawant and M. H. Cho, *RSC Adv.*, 2015, **5**, 97788–97797.

55 A. Kotkin, V. Kochergin, E. Kabachkov, Y. Shulga, A. Lobach, R. Manzhos and A. Krivenko, *Mater. Today Energy*, 2020, **17**, 100459.

56 J. Liu, M. Notarianni, G. Will, V. T. Tiong, H. Wang and N. Motta, *Langmuir*, 2013, **29**, 13307–13314.

57 K. Parvez, Z.-S. Wu, R. Li, X. Liu, R. Graf, X. Feng and K. Müllen, *J. Am. Chem. Soc.*, 2014, **136**, 6083–6091.

58 K. S. Rao, J. Senthilnathan, Y.-F. Liu and M. Yoshimura, *Sci. Rep.*, 2014, **4**, 4237.

59 N. Liu, F. Luo, H. Wu, Y. Liu, C. Zhang and J. Chen, *Adv. Funct. Mater.*, 2008, **18**, 1518–1525.

60 A. Gutiérrez-Cruz, A. R. Ruiz-Hernández, J. F. Vega-Clemente, D. G. Luna-Gazcón and J. Campos-Delgado, *J. Mater. Sci.*, 2022, **57**, 14543–14578.

61 T. D. Dao and H. M. Jeong, *Mater. Res. Bull.*, 2015, **70**, 651–657.

62 F. Amato, I. Ferrari, A. Motta, R. Zanoni, E. A. Dalchiele and A. G. Marrani, *RSC Adv.*, 2023, **13**, 29308–29315.

63 G. Kumar, S. Mishra, F. Yang and S. Kundalwal, *J. Mater. Sci.*, 2025, 1–57.

64 L. G. Guex, B. Sacchi, K. F. Peuvot, R. L. Andersson, A. M. Pourrahimi, V. Ström, S. Farris and R. T. Olsson, *Nanoscale*, 2017, **9**, 9562–9571.

65 T. Zhou, F. Chen, K. Liu, H. Deng, Q. Zhang, J. Feng and Q. Fu, *Nanotechnology*, 2010, **22**, 045704.

66 A. A. Bayode, M. T. Folorunso, B. Helmreich and M. O. Omorogie, *ACS Omega*, 2023, **8**, 7956–7967.

67 O. E.-B. Hassan, Y. Chenavier, V. Maurel, J. Pérard, A. Bouzina, L. Dubois and F. Duclairoir, *Mater. Adv.*, 2025, **6**, 143–147.

68 Z. Khosroshahi, M. Kharaziha, F. Karimzadeh and A. Allafchian, *AIP Conf. Proc.*, 2018, **1920**(1), 020009.

69 S. S. Emmanuel, C. O. Olawoyin, A. A. Adesibikan, S. A. Nafiu and A. A. Bayode, *J. Organomet. Chem.*, 2024, **1005**, 122984.

70 S. S. Emmanuel and A. A. Adesibikan, *Water Environ. Res.*, 2021, **93**, 2873–2882.

71 S. S. Emmanuel, A. A. Adesibikan, C. Olusola Olawoyin and A. A. Bayode, *ChemistrySelect*, 2023, **8**, e202302712.

72 S. S. Emmanuel, A. A. Adesibikan, E. A. Opatola and C. O. Olawoyin, *Appl. Organomet. Chem.*, 2023, **37**, e7108.

73 M. Khan, A. H. Al-Marri, M. Khan, N. Mohri, S. F. Adil, A. Al-Warthan, M. R. H. Siddiqui, H. Z. Alkhathlan, R. Berger and W. Tremel, *RSC Adv.*, 2014, **4**, 24119–24125.

74 O. O. Oluwaniyi, A. A. Adesibikan and S. S. Emmanuel, *ChemistrySelect*, 2022, **7**, e202200711.

75 J. O. Oladipo, O. O. Oluwaniyi, S. S. Emmanuel, B. T. Oyewo, G. V. Awolola, S. A. Oyeyinka and O. A. Omole, *Agric. Conspectus Sci.*, 2023, **88**, 103–108.

76 K. O. Iwuozor, S. S. Emmanuel, M. O. Ahmed, A. M. Idris, E. C. Emenike, O. D. Saliu, A. H. Qudus and A. G. Adeniyi, *Chem. Afr.*, 2024, **7**, 539–563.

77 S. S. Emmanuel, A. A. Adesibikan and O. D. Saliu, *Appl. Organomet. Chem.*, 2023, **37**, e6946.

78 S. S. Emmanuel, M. O. Idris, C. O. Olawoyin, A. A. Adesibikan, A. A. Aliyu and A. I. Suleiman, *ChemistrySelect*, 2024, **9**, e202304956.

79 M. Yi and Z. Shen, *J. Mater. Chem. A*, 2015, **3**, 11700–11715.

80 W. Zhao, M. Fang, F. Wu, H. Wu, L. Wang and G. Chen, *J. Mater. Chem.*, 2010, **20**, 5817–5819.

81 Y. Lv, L. Yu, C. Jiang, S. Chen and Z. Nie, *RSC Adv.*, 2014, **4**, 13350–13354.

82 T. Lin, Y. Tang, Y. Wang, H. Bi, Z. Liu, F. Huang, X. Xie and M. Jiang, *Energy Environ. Sci.*, 2013, **6**, 1283–1290.

83 N. Arora and N. N. Sharma, *Diamond Relat. Mater.*, 2014, **50**, 135–150.

84 X. Wu, Y. Liu, H. Yang and Z. Shi, *RSC Adv.*, 2016, **6**, 93119–93124.

85 H. Tan, D. Wang and Y. Guo, *Materials*, 2019, **12**, 2279.

86 G.-W. Cheng, K. Chu, J. S. Chen and J. T. H. Tsai, *Superlattices Microstruct.*, 2017, **104**, 258–265.

87 C. Wu, G. Dong and L. Guan, *Phys. E*, 2010, **42**, 1267–1271.

88 S. Kim, Y. Song, J. Wright and M. J. Heller, *Carbon*, 2016, **102**, 339–345.

89 B. Qin, T. Zhang, H. Chen and Y. Ma, *Carbon*, 2016, **102**, 494–498.

90 Y. Su and Y. Zhang, *Carbon*, 2015, **83**, 90–99.

91 R. Goyat, Y. Saharan, J. Singh, A. Umar and S. Akbar, *Molecules*, 2022, **27**, 6433.

92 M. S. A. Bhuyan, M. N. Uddin, M. M. Islam, F. A. Bipasha and S. S. Hossain, *Int. Nano Lett.*, 2016, **6**, 65–83.

93 A. A. Adesibikan, S. S. Emmanuel, C. O. Olawoyin and P. Ndungu, *J. Organomet. Chem.*, 2024, **1010**, 123087.

94 A. Poniatowska, M. Trzaskowski and T. Ciach, *Colloids Surf., A*, 2019, **561**, 315–324.

95 A. O. Adeola and P. B. C. Forbes, *Water Sci. Technol.*, 2020, **80**, 1931–1943.

96 S. S. Emmanuel, C. O. Olawoyin, A. A. Adesibikan and E. A. Opatola, *J. Polym. Environ.*, 2024, **32**, 1–30.

97 B. Vasić, U. Ralević, K. C. Zobenica, M. M. Smiljanić, R. Gajić, M. Spasenović and S. Vollebregt, *Appl. Surf. Sci.*, 2020, **509**, 144792.

98 C.-M. Seah, S.-P. Chai and A. R. Mohamed, *Carbon*, 2014, **70**, 1–21.

99 Y. Du, J. Su, W. Luo and G. Cheng, *ACS Appl. Mater. Interfaces*, 2015, **7**, 1031–1034.

100 S. Cai, X. Chen, P. Liu, H. Zhou, S. Fu, K. Xu, S. Chen and D. Liang, *J. Mater. Eng. Perform.*, 2020, **29**, 2248–2255.

101 Z. Chen, W. Ren, L. Gao, B. Liu, S. Pei and H.-M. Cheng, *Nat. Mater.*, 2011, **10**, 424–428.

102 X. Dong, X. Wang, L. Wang, H. Song, H. Zhang, W. Huang and P. Chen, *ACS Appl. Mater. Interfaces*, 2012, **4**, 3129–3133.

103 M. T. Pettes, H. Ji, R. S. Ruoff and L. Shi, *Nano Lett.*, 2012, **12**, 2959–2964.

104 Z. Liu, Z. Tu, Y. Li, F. Yang, S. Han, W. Yang, L. Zhang, G. Wang, C. Xu and J. Gao, *Mater. Lett.*, 2014, **122**, 285–288.

105 B.-J. Kim, G. Yang, M. Joo Park, J. Seop Kwak, K. Hyeon Baik, D. Kim and J. Kim, *Appl. Phys. Lett.*, 2013, **102**(16), 161902.

106 D. Xia, K. Yi, B. Zheng, M. Li, G. Qi, Z. Cai, M. Cao, D. Liu, L. Peng and D. Wei, *J. Phys. Chem. C*, 2017, **121**, 3062–3069.

107 S. Lee, W. K. Park, Y. Yoon, B. Baek, J. S. Yoo, S. B. Kwon, D. H. Kim, Y. J. Hong, B. K. Kang and D. H. Yoon, *Mater. Sci. Eng., B*, 2019, **242**, 63–68.

108 L. Shi, K. Chen, R. Du, A. Bachmatiuk, M. H. Rümmeli, K. Xie, Y. Huang, Y. Zhang and Z. Liu, *J. Am. Chem. Soc.*, 2016, **138**, 6360–6363.

109 M. Xu, D. Fujita, K. Sagisaka, E. Watanabe and N. Hanagata, *ACS Nano*, 2011, **5**, 1522–1528.

110 S. Bhaviripudi, X. Jia, M. S. Dresselhaus and J. Kong, *Nano Lett.*, 2010, **10**, 4128–4133.

111 S. Bae, H. K. Kim, Y. Lee, X. Xu, J.-S. Park, Y. Zheng, J. Balakrishnan, T. Lei, H. R. Kim, Y. I. Song, Y. J. Kim, K. S. Kim, B. Özyilmaz, J.-H. Ahn, B. H. Hong and S. Iijima, *Nat. Nanotechnol.*, 2010, **5**, 574–578.

112 K. T. Young, C. Smith, T. M. Krentz, D. A. Hitchcock and E. M. Vogel, *Carbon*, 2021, **176**, 106–117.

113 C. Berger, Z. Song, T. Li, X. Li, A. Y. Ogbazghi, R. Feng, Z. Dai, A. N. Marchenkov, E. H. Conrad and P. N. First, *J. Phys. Chem. B*, 2004, **108**, 19912–19916.

114 E. Rollings, G.-H. Gweon, S. Zhou, B. Mun, J. McChesney, B. Hussain, A. Fedorov, P. First, W. De Heer and A. Lanzara, *J. Phys. Chem. Solids*, 2006, **67**, 2172–2177.

115 B. Deng, Z. Xin, R. Xue, S. Zhang, X. Xu, J. Gao, J. Tang, Y. Qi, Y. Wang and Y. Zhao, *Sci. Bull.*, 2019, **64**, 659–668.

116 K. V. Emtsev, A. Bostwick, K. Horn, J. Jobst, G. L. Kellogg, L. Ley, J. L. McChesney, T. Ohta, S. A. Reshanov and J. Röhrl, *Nat. Mater.*, 2009, **8**, 203–207.

117 W. A. De Heer, C. Berger, M. Ruan, M. Sprinkle, X. Li, Y. Hu, B. Zhang, J. Hankinson and E. Conrad, *Proc. Natl. Acad. Sci. U. S. A.*, 2011, **108**, 16900–16905.

118 R. Tromp and J. Hannon, *Phys. Rev. Lett.*, 2009, **102**, 106104.

119 J. Wu, W. Pisula and K. Müllen, *Chem. Rev.*, 2007, **107**, 718–747.

120 L. Chen, Y. Hernandez, X. Feng and K. Müllen, *Angew. Chem., Int. Ed.*, 2012, **51**, 7640–7654.

121 W. Yang, A. Lucotti, M. Tommasini and W. A. Chalifoux, *J. Am. Chem. Soc.*, 2016, **138**, 9137–9144.

122 M. Treier, C. A. Pignedoli, T. Laino, R. Rieger, K. Müllen, D. Passerone and R. Fasel, *Nat. Chem.*, 2011, **3**, 61–67.

123 X. Yang, X. Dou, A. Rouhanipour, L. Zhi, H. J. Räder and K. Müllen, *J. Am. Chem. Soc.*, 2008, **130**, 4216–4217.

124 A. Sinitskii, A. A. Fursina, D. V. Kosynkin, A. L. Higginbotham, D. Natelson and J. M. Tour, *Appl. Phys. Lett.*, 2009, **95**(25), 253108.

125 J. Wu, Ž. Tomović, V. Enkelmann and K. Müllen, *J. Org. Chem.*, 2004, **69**, 5179–5186.

126 H. Tsao, H. J. Räder, W. Pisula, A. Rouhanipour and K. Müllen, *Phys. Status Solidi*, 2008, **205**, 421–429.

127 Z. Sun, Z. Yan, J. Yao, E. Beitler, Y. Zhu and J. M. Tour, *Nature*, 2010, **468**, 549–552.

128 S. S. Emmanuel, C. O. Olawoyin, I. D. Ayodele and O. J. Oluwole, *J. Organomet. Chem.*, 2023, **996**, 122767.

129 R. Ye and J. M. Tour, *ACS Nano*, 2019, **13**, 10872–10878.

130 J. Sha, Y. Li, R. Villegas Salvatierra, T. Wang, P. Dong, Y. Ji, S.-K. Lee, C. Zhang, J. Zhang and R. H. Smith, *ACS Nano*, 2017, **11**, 6860–6867.

131 J. Lin, Z. Peng, Y. Liu, F. Ruiz-Zepeda, R. Ye, E. L. Samuel, M. J. Yacaman, B. I. Yakobson and J. M. Tour, *Nat. Commun.*, 2014, **5**, 5714.

132 M. G. Stanford, C. Zhang, J. D. Fowlkes, A. Hoffman, I. N. Ivanov, P. D. Rack and J. M. Tour, *ACS Appl. Mater. Interfaces*, 2020, **12**, 10902–10907.

133 R. Ye, D. K. James and J. M. Tour, *Accounts Chem. Res.*, 2018, **51**, 1609–1620.

134 B. Kulyk, B. F. Silva, A. F. Carvalho, S. Silvestre, A. J. Fernandes, R. Martins, E. Fortunato and F. M. Costa, *ACS Appl. Mater. Interfaces*, 2021, **13**, 10210–10221.

135 J. L. Beckham, J. T. Li, M. G. Stanford, W. Chen, E. A. McHugh, P. A. Advincula, K. M. Wyss, Y. Chyan, W. L. Boldman and P. D. Rack, *ACS Nano*, 2021, **15**, 8976–8983.

136 M. Jalili, H. Ghanbari, S. M. Bellah and R. Malekfar, *J. Mater. Sci. Technol.*, 2019, **35**, 292–299.

137 M. Qian, Y. S. Zhou, Y. Gao, J. B. Park, T. Feng, S. M. Huang, Z. Sun, L. Jiang and Y. F. Lu, *Appl. Phys. Lett.*, 2011, **98**(17), 173108.

138 G. R. Kiran, B. Chandu, S. G. Acharyya, S. V. Rao and V. V. Srikanth, *Philos. Mag. Lett.*, 2017, **97**, 229–234.

139 P. Nancy, J. Jose, N. Joy, S. Valluvadasan, R. Philip, R. Antoine, S. Thomas and N. Kalarikkal, *Nanomaterials*, 2021, **11**, 880.

140 P. Russo, A. Hu, G. Compagnini, W. W. Duley and N. Y. Zhou, *Nanoscale*, 2014, **6**, 2381–2389.

141 R. Ye, D. K. James and J. M. Tour, *Adv. Mater.*, 2019, **31**, 1803621.

142 I. Manisalidis, E. Stavropoulou, A. Stavropoulos and E. Bezirtzoglou, *Front. Public Health*, 2020, **8**, 505570.

143 G.-P. Bǎlǎ, R.-M. Râjnoveanu, E. Tudorache, R. Motişan and C. Oancea, *Environ. Sci. Pollut. Res.*, 2021, **28**, 19615–19628.

144 N. K. Shammas, L. K. Wang and M.-H. S. Wang, in *Handbook of Environment and Waste Management: Acid Rain and Greenhouse Gas Pollution Control*, World Scientific, 2020, pp. 1–26.

145 R. Pandey and B. Chandrashekhar, *Crit. Rev. Environ. Sci. Technol.*, 2014, **44**, 34–96.

146 Z. ur Rahman, X. Wang, J. Zhang, Z. Yang, G. Dai, P. Verma, H. Mikulcic, M. Vujanovic, H. Tan and R. L. Axelbaum, *Renew. Sustain. Energy Rev.*, 2022, **157**, 112020.

147 X. Wang, Y. Qin, L. Zhu and H. Tang, *Environ. Sci. Technol.*, 2015, **49**, 6855–6864.

148 S. Yu, X. Wang, Y. Ai, X. Tan, T. Hayat, W. Hu and X. Wang, *J. Mater. Chem. A*, 2016, **4**, 5654–5662.

149 L. Yu, L. Wang, W. Xu, L. Chen, M. Fu, J. Wu and D. Ye, *J. Environ. Sci.*, 2018, **67**, 171–178.

150 M. Aivalioti, I. Vamvasakis and E. Gidarakos, *J. Hazard. Mater.*, 2010, **178**, 136–143.

151 C.-F. Wu, S.-Y. Wu, Y.-H. Wu, A. C. Cullen, T. V. Larson, J. Williamson and L.-J. S. Liu, *Environ. Int.*, 2009, **35**, 516–522.

152 G. B. Baur, O. Beswick, J. Spring, I. Yuranov and L. Kiwi-Minsker, *Adsorption*, 2015, **21**, 255–264.

153 M. Lillo-Ródenas, D. Cazorla-Amorós and A. Linares-Solano, *Carbon*, 2005, **43**, 1758–1767.

154 S. Wang, H. Sun, H.-M. Ang and M. O. Tadé, *Chem. Eng. J.*, 2013, **226**, 336–347.

155 F. Chu, Y. Zheng, B. Wen, L. Zhou, J. Yan and Y. Chen, *RSC Adv.*, 2018, **8**, 2426–2432.

156 J. M. Kim, J. H. Kim, C. Y. Lee, D. W. Jerng and H. S. Ahn, *J. Hazard Mater.*, 2018, **344**, 458–465.

157 R. Shadkam, M. Naderi, A. Ghazitabar and S. Akbari, *Mater. Today Commun.*, 2021, **28**, 102610.

158 M. B. Hosseinabadi and A. F. Zarandi, *Anal. Methods Environ. Chem. J.*, 2019, **2**, 45–54.

159 Y. Dai, M. Li, F. Liu, M. Xue, Y. Wang and C. Zhao, *Environ. Sci. Pollut. Res.*, 2019, **26**, 2477–2491.

160 B. Szczęśniak, Ł. Osuchowski, J. Choma and M. Jaroniec, *J. Porous Mater.*, 2018, **25**, 621–627.

161 B. Szczęśniak, J. Choma and M. Jaroniec, *Microporous Mesoporous Mater.*, 2018, **261**, 105–110.

162 S. T. Lim, J. H. Kim, C. Y. Lee, S. Koo, D.-W. Jerng, S. Wongwises and H. S. Ahn, *Sci. Rep.*, 2019, **9**, 10922.

163 Y. Wang, Z. Li, C. Tang, H. Ren, Q. Zhang, M. Xue, J. Xiong, D. Wang, Q. Yu and Z. He, *Environ. Sci.: Nano*, 2019, **6**, 3113–3122.

164 G.-Q. Liu, M.-X. Wan, Z.-H. Huang and F.-Y. Kang, *N. Carbon Mater.*, 2015, **30**, 566–571.

165 T. T. N. Vo, S. T. Lim, J. H. Kim, G. H. Shim, K. M. Kim, B. Kweon, M. Kim, C. Y. Lee and H. S. Ahn, *RSC Adv.*, 2022, **12**, 14570–14577.

166 R. Mishra, A. Kumar, E. Singh, A. Kumari and S. Kumar, *Process Saf. Environ. Prot.*, 2023, **180**, 800–807.

167 J. Cheng, S. Tang, Z. Lin, Z. Wang, D. Wu, D. Wang, C. Liu and Z. Cao, *Appl. Surf. Sci.*, 2024, **648**, 159073.

168 P. Lazar, F. Karlicky, P. Jurecka, M. S. Kocman, E. Otyepková, K. R. Šafářová and M. Otyepka, *J. Am. Chem. Soc.*, 2013, **135**, 6372–6377.

169 Y.-H. Shih and M.-S. Li, *J. Hazard Mater.*, 2008, **154**, 21–28.

170 E. R. Gil, B. Ruiz, M. Lozano, M. Martín and E. Fuente, *Chem. Eng. J.*, 2014, **245**, 80–88.

171 F.-Y. Yi, X.-D. Lin, S.-X. Chen and X.-Q. Wei, *J. Porous Mater.*, 2009, **16**, 521–526.

172 Y. Tao, D. Kong, C. Zhang, W. Lv, M. Wang, B. Li, Z.-H. Huang, F. Kang and Q.-H. Yang, *Carbon*, 2014, **69**, 169–177.

173 J. Lee, M. Kang, I.-K. Shim, D. H. Lee, A. Kim and H. Jung, *J. Nanosci. Nanotechnol.*, 2018, **18**, 6995–7003.

174 Y. Shen, X. Zhu, L. Zhu and B. Chen, *Chem. Eng. J.*, 2017, **314**, 336–346.

175 C. Tang, B. Q. Li, Q. Zhang, L. Zhu, H. F. Wang, J. L. Shi and F. Wei, *Adv. Funct. Mater.*, 2016, **26**, 577–585.

176 Z. Yang, S. Chabi, Y. Xia and Y. Zhu, *Prog. Nat. Sci. Mater. Int.*, 2015, **25**, 554–562.

177 J. L. Shi, C. Tang, H. J. Peng, L. Zhu, X. B. Cheng, J. Q. Huang, W. Zhu and Q. Zhang, *Small*, 2015, **11**, 5243–5252.

178 K. Rahbar Shamskar, A. Rashidi, P. Aberoomand Azar, M. Yousefi and S. Baniyaghoob, *Environ. Sci. Pollut. Res.*, 2019, **26**, 3643–3650.

179 X. Chen and B. Chen, *Environ. Sci. Technol.*, 2015, **49**, 6181–6189.

180 Y. Su, Z. Ao, Y. Ji, G. Li and T. An, *Appl. Surf. Sci.*, 2018, **450**, 484–491.

181 V. Verdinelli, E. Germán, C. R. Luna, J. M. Marchetti, M. A. Volpe and A. Juan, *J. Phys. Chem. C*, 2014, **118**, 27672–27680.

182 Z. Ao, S. Dou, Z. Xu, Q. Jiang and G. Wang, *Int. J. Hydrogen Energy*, 2014, **39**, 16244–16251.

183 B. Liu, W. Zhao, Q. Jiang, Z. Ao and T. An, *Sustain. Mater. Technol.*, 2019, **21**, e00103.

184 R. Zhang, J. Jing, J. Tao, S.-C. Hsu, G. Wang, J. Cao, C. S. L. Lee, L. Zhu, Z. Chen and Y. Zhao, *Atmos. Chem. Phys.*, 2013, **13**, 7053–7074.

185 D. E. Horton, C. B. Skinner, D. Singh and N. S. Diffenbaugh, *Nat. Clim. Change*, 2014, **4**, 698–703.

186 L. P. Naeher, K. R. Smith, B. Leaderer, L. Neufeld and D. Mage, *Environ. Sci. Technol.*, 2001, **35**, 575–581.

187 S. C. Anenberg, L. W. Horowitz, D. Q. Tong and J. J. West, *Environ. Health Perspect.*, 2010, **118**, 1189–1195.

188 G. Zhu, T. Chen, Y. Hu, L. Ma, R. Chen, H. Lv, Y. Wang, J. Liang, X. Li and C. Yan, *Nano Energy*, 2017, **33**, 229–237.

189 W. Jung, J. S. Lee, S. Han, S. H. Ko, T. Kim and Y. H. Kim, *J. Mater. Chem. A*, 2018, **6**, 16975–16982.

190 J. Liang, C. Yuan, H. Li, K. Fan, Z. Wei, H. Sun and J. Ma, *Nano-Micro Lett.*, 2018, **10**, 1–9.

191 S. Zhang, H. Liu, F. Zuo, X. Yin, J. Yu and B. Ding, *Small*, 2017, **13**, 1603151.

192 H. Dai, X. Liu, C. Zhang, K. Ma and Y. Zhang, *Sep. Purif. Technol.*, 2021, **276**, 119243.

193 P. Zhang, D. Wan, Z. Zhang, G. Wang, J. Hu and G. Shao, *Environ. Sci.: Nano*, 2018, **5**, 1813–1820.

194 S. Yan, G. Zhang, F. Li, L. Zhang, S. Wang, H. Zhao, Q. Ge and H. Li, *Nanoscale*, 2019, **11**, 10372–10380.

195 W. Zou, B. Gu, S. Sun, S. Wang, X. Li, H. Zhao and P. Yang, *Mater. Res. Express*, 2019, **6**, 105624.

196 F. Leach, G. Kalghatgi, R. Stone and P. Miles, *J. Transport. Eng.*, 2020, **1**, 100005.

197 A. Trapalis, N. Todorova, T. Giannakopoulou, N. Boukos, T. Speliotis, D. Dimotikali and J. Yu, *Appl. Catal., B*, 2016, **180**, 637–647.

198 H. Gao and Z. Liu, *RSC Adv.*, 2017, **7**, 13082–13091.

199 J. Ni, M. Quintana and S. Song, *Phys. E*, 2020, **116**, 113768.

200 A. S. Rad, A. Shadravan, A. A. Soleymani and N. Motaghedi, *Curr. Appl. Phys.*, 2015, **15**, 1271–1277.

201 L. Ferrighi, M. Datteo and C. Di Valentin, *J. Phys. Chem. C*, 2014, **118**, 223–230.

202 T. Wehling, M. Katsnelson and A. Lichtenstein, *Chem. Phys. Lett.*, 2009, **476**, 125–134.

203 T. O. Wehling, A. I. Lichtenstein and M. I. Katsnelson, *Appl. Phys. Lett.*, 2008, **93**(20), 202110.

204 S. Seenithurai, R. K. Pandyan, S. V. Kumar, C. Saranya and M. Mahendran, *Int. J. Hydrogen Energy*, 2014, **39**, 11990–11998.

205 A. Ahmadi Peyghan, N. L. Hadipour and Z. Bagheri, *J. Phys. Chem. C*, 2013, **117**, 2427–2432.

206 A. A. Peyghan, M. Noei and S. Yourdkhani, *Superlattices Microstruct.*, 2013, **59**, 115–122.

207 A. S. Rad, *Appl. Surf. Sci.*, 2015, **357**, 1217–1224.

208 G. Rajasekaran and A. Parashar, *Mater. Today: Proc.*, 2018, **5**, 6780–6788.

209 L. Vicarelli, S. J. Heerema, C. Dekker and H. W. Zandbergen, *ACS Nano*, 2015, **9**, 3428–3435.

210 M. Shakourian-Fard and G. Kamath, *Phys. Chem. Chem. Phys.*, 2017, **19**, 4383–4395.

211 M. Ali, X. Pi, Y. Liu and D. Yang, *AIP Adv.*, 2017, **7**(4), 045308.

212 Y. You, J. Deng, X. Tan, N. Gorjizadeh, M. Yoshimura, S. Smith, V. Sahajwalla and R. Joshi, *Phys. Chem. Chem. Phys.*, 2017, **19**, 6051–6056.

213 N. M. Caffrey, R. Armiento, R. Yakimova and I. A. Abrikosov, *Phys. Rev. B*, 2016, **94**, 205411.

214 Y.-H. Zhang, Y.-B. Chen, K.-G. Zhou, C.-H. Liu, J. Zeng, H.-L. Zhang and Y. Peng, *Nanotechnology*, 2009, **20**, 185504.

215 A. K. Mishra and S. Ramaprabhu, *Energy Environ. Sci.*, 2011, **4**, 889–895.

216 A. K. Mishra and S. Ramaprabhu, *J. Appl. Phys.*, 2014, **116**(6), 064306.

217 M. Ali and N. Tit, *Surf. Sci.*, 2019, **684**, 28–36.

218 Y. Zhu, S. Murali, W. Cai, X. Li, J. W. Suk, J. R. Potts and R. S. Ruoff, *Adv. Mater.*, 2010, **22**, 3906–3924.

219 S. S. Varghese, S. Lonkar, K. Singh, S. Swaminathan and A. Abdala, *Sens. Actuators, B*, 2015, **218**, 160–183.

220 B. Cho, J. Yoon, M. G. Hahm, D.-H. Kim, A. R. Kim, Y. H. Kahng, S.-W. Park, Y.-J. Lee, S.-G. Park and J.-D. Kwon, *J. Mater. Chem. C*, 2014, **2**, 5280–5285.

221 O. Leenaerts, B. Partoens and F. Peeters, *Phys. Rev. B: Condens. Matter Mater. Phys.*, 2008, **77**, 125416.

222 Q. Tang, Z. Zhou and Z. Chen, *Nanoscale*, 2013, **5**, 4541–4583.

223 X.-Y. Liang, N. Ding, S.-P. Ng and C.-M. L. Wu, *Appl. Surf. Sci.*, 2017, **411**, 11–17.

224 C. Chen, K. Xu, X. Ji, L. Miao and J. Jiang, *Phys. Chem. Chem. Phys.*, 2014, **16**, 11031–11036.

225 D. Cortés-Arriagada and N. Villegas-Escobar, *Appl. Surf. Sci.*, 2017, **420**, 446–455.

226 S. U. D. Shamim, D. Roy, S. Alam, A. A. Piya, M. S. Rahman, M. K. Hossain and F. Ahmed, *Appl. Surf. Sci.*, 2022, **596**, 153603.

227 A. Tiwari, J. Palepu, A. Choudhury, S. Bhattacharya and S. Kanungo, *FlatChem*, 2022, **34**, 100392.

228 M. M. Husain, M. T. Ansari and A. Almohammedi, *Mater. Today Commun.*, 2024, **39**, 108725.

229 R. Pan, Y. Tang, Y. Guo, J. Shang, L. Zhou, W. Dong and D. He, *Microporous Mesoporous Mater.*, 2021, **323**, 111197.

230 X. Gao, Q. Zhou, J. Wang, L. Xu and W. Zeng, *Appl. Surf. Sci.*, 2020, **517**, 146180.

231 Z. Karami, A. Hamed Mashhadzadeh, S. Habibzadeh, M. R. Ganjali, E. M. Ghardi, A. Hasnaoui, V. Vatanpour, G. Sharma, A. Esmaeili, F. J. Stadler and M. R. Saeb, *J. Mol. Model.*, 2021, **27**, 70.

232 Q. Luo, S. Yin, X. Sun, Y. Tang, Z. Feng and X. J. M. Dai, *Nanostructures*, 2022, **171**, 207401.

233 H. Zhang, W. Cen, J. Liu, J. Guo, H. Yin and P. Ning, *Appl. Surf. Sci.*, 2015, **324**, 61–67.

234 Z. Zhang, B. Liang, Y. Chi, Y. Jiang, J. Song and Y. Guo, *Superlattices Microstruct.*, 2021, **159**, 107036.

235 X. Yan, T. Shen, X. Liu, C. Liu and A. Gong, *Solid State Commun.*, 2023, **369**, 115196.

236 A. O. Adeola, A. S. Akingboye, O. T. Ore, O. A. Oluwajana, A. H. Adewole, D. B. Olawade and A. C. Ogunyele, *Environ. Syst. Decis.*, 2022, **42**, 26–50.

237 Q. Hassan, P. Viktor, T. J. Al-Musawi, B. Mahmood Ali, S. Algburi, H. M. Alzoubi, A. Khudhair Al-Jiboory, A. Zuhair Sameen, H. M. Salman and M. Jaszczur, *Renew. Energy Focus*, 2024, **48**, 100545.

238 C. Y. Chuah, J. Lee, J. Song and T.-H. Bae, *Membranes*, 2021, **11**, 284.

239 P. Z. Sun, M. Yagmurcukardes, R. Zhang, W. J. Kuang, M. Lozada-Hidalgo, B. L. Liu, H. M. Cheng, F. C. Wang, F. M. Peeters, I. V. Grigorieva and A. K. Geim, *Nat. Commun.*, 2021, **12**, 7170.

240 L. Huang, W. Jia and H. Lin, *AIChE J.*, 2020, **66**, e17022.

241 F. Malekian, H. Ghafourian, K. Zare, A. A. Sharif and Y. Zamani, *Eur. Phys. J. Plus.*, 2019, **134**, 212.

242 S. Singh, M. R. Hasan, P. Sharma and J. Narang, *Sens. Int.*, 2022, **3**, 100190.

243 R. Casadei, M. Giacinti Baschetti, M. J. Yoo, H. B. Park and L. Giorgini, *Membranes*, 2020, **10**, 188.

244 B. E. Arango Hoyos, H. F. Osorio, E. K. Valencia Gómez, J. Guerrero Sánchez, A. P. Del Canto Palominos, F. A. Larrain and J. J. Prías Barragán, *Sci. Rep.*, 2023, **13**, 14476.

245 K. R. Chaturvedi and T. Sharma, in *Nanotechnology for CO₂ Utilization in Oilfield Applications*, ed. T. Sharma, K. R. Chaturvedi and J. J. Trivedi, Gulf Professional Publishing, 2022, pp. 71–84, DOI: 10.1016/B978-0-323-90540-4.00011-9.

246 X. Hu, X. Yang, L. Chen, M. Mei, Z. Song, Z. Fei, P. J. Dyson and Z. Qi, *Chem. Eng. J.*, 2022, **435**, 134956.

247 R. B. de Oliveira, D. D. Borges and L. D. Machado, *Sci. Rep.*, 2022, **12**, 22393.

248 M. Khraisheh, F. Almomani and G. Walker, *Sci. Rep.*, 2020, **10**, 269.

249 S. Yousef, J. Šereika, A. Tonkonogovas, T. Hashem and A. Mohamed, *Environ. Technol. Innovat.*, 2021, **21**, 101339.

250 S. Yun, H. Lee, W.-E. Lee and H. S. Park, *Fuel*, 2016, **174**, 36–42.

251 K. Xia, R. Xiong, Y. Chen, D. Liu, Q. Tian, Q. Gao, B. Han and C. Zhou, *Colloids Surf., A*, 2021, **622**, 126640.

252 L.-Y. Meng and S.-J. Park, *J. Colloid Interface Sci.*, 2010, **352**, 498–503.

253 A. K. Mishra and S. Ramaprabhu, *AIP Adv.*, 2011, **1**, 032152.

254 S. Chowdhury, G. K. Parshetti and R. Balasubramanian, *Chem. Eng. J.*, 2015, **263**, 374–384.

255 W. Li, X. Jiang, H. Yang and Q. Liu, *Appl. Surf. Sci.*, 2015, **356**, 812–816.

256 Y. Hosseini, M. Najafi, S. Khalili, M. Jahanshahi and M. Peyravi, *Mater. Chem. Phys.*, 2021, **270**, 124788.

257 A. Pruna, A. C. Cárcel, A. Benedito and E. Giménez, *Appl. Surf. Sci.*, 2019, **487**, 228–235.

258 N. Hsan, P. K. Dutta, S. Kumar, R. Bera and N. Das, *Int. J. Biol. Macromol.*, 2019, **125**, 300–306.

259 L. An, S. Liu, L. Wang, J. Wu, Z. Wu, C. Ma, Q. Yu and X. Hu, *Ind. Eng. Chem. Res.*, 2019, **58**, 3349–3358.

260 S. Chowdhury and R. Balasubramanian, *Ind. Eng. Chem. Res.*, 2016, **55**, 7906–7916.

261 S. Ullah, M. A. Bustam, A. G. Al-Sehemi, M. A. Assiri, F. A. Abdul Kareem, A. Mukhtar, M. Ayoub and G. Gonfa, *Microporous Mesoporous Mater.*, 2020, **296**, 110002.

262 B. Szczęśniak and J. Choma, *Microporous Mesoporous Mater.*, 2020, **292**, 109761.

263 S. Shang, Z. Tao, C. Yang, A. Hanif, L. Li, D. C. W. Tsang, Q. Gu and J. Shang, *Chem. Eng. J.*, 2020, **393**, 124666.

264 A. M. Varghese, K. S. K. Reddy, N. Bhoria, S. Singh, J. Pokhrel and G. N. Karanikolos, *Chem. Eng. J.*, 2021, **420**, 129677.

265 Y. Cao, Y. Zhao, Z. Lv, F. Song and Q. Zhong, *J. Ind. Eng. Chem.*, 2015, **27**, 102–107.

266 N. Politakos, I. Barbarin, T. Cordero-Lanzac, A. Gonzalez, R. Zangi and R. Tomovska, *Polymers*, 2020, **12**, 936.

267 S. Rodríguez-García, R. Santiago, D. López-Díaz, M. D. Merchán, M. M. Velázquez, J. L. G. Fierro and J. Palomar, *ACS Sustain. Chem. Eng.*, 2019, **7**, 12464–12473.

268 C. A. Gunathilake, G. G. T. A. Ranathunge, R. S. Dassanayake, S. D. Illesinghe, A. S. Manchanda, C. S. Kalpage, R. M. G. Rajapakse and D. G. G. P. Karunaratne, *Environ. Sci.: Nano*, 2020, **7**, 1225–1239.

269 S. Stanly, E. J. Jelmy, C. P. R. Nair and H. John, *J. Environ. Chem. Eng.*, 2019, **7**, 103344.